NASA
IN-72
361048

DEPARTMENT OF MATHMATICS AND STATISTICS
COLLEGE OF SCIENCES
OLD DOMINION UNIVERSITY
NORFOLK, VIRGINIA 23529-0247

A MULTIGROUP METHOD FOR THE CALCULATION OF NEUTRON FLUENCE WITH A SOURCE TERM

By
Dr. J. H. Heinbockel, Principal Investigator
And
M. S. Clowdsley, Graduate Student
Department of Mathematics and Statistics

FINAL REPORT
For the period ending September 30, 1998

August 1998

Old Dominion University Research Foundation

DEPARTMENT OF MATHMATICS AND STATISTICS
COLLEGE OF SCIENCES
OLD DOMINION UNIVERSITY
NORFOLK, VIRGINIA 23529-0247

A MULTIGROUP METHOD FOR THE CALCULATION OF NEUTRON FLUENCE WITH A SOURCE TERM

By
Dr. J. H. Heinbockel, Principal Investigator
And
M. S. Clowdsley, Graduate Student
Department of Mathematics and Statistics

FINAL REPORT
For the period ending September 30, 1998

August 1998

FINAL REPORT RESEARCH GRANT NCC 1-42

A Multigroup Method for the Calculation of Neutron Fluence with a Source Term

by J.H. Heinbockel*, M.S. Clowdsley**

*Professor, Old Dominion University, Norfolk, VA 23529-0077, U.S.A.

**Graduate Student, Old Dominion University, Norfolk, VA 23529-0077, U.S.A.

Introduction

Previous accomplishments resulting from the research Grant NCC 1-42 have been numerous. These accomplishments are summarized in the appendices A,B and C of this report. The Appendix A lists publications that have resulted from the varied research efforts associated with this grant. The Appendix B lists graduate students who have been associated with this grant, their research efforts and their degree accomplishments. The Appendix C is a summary of efforts involving Green's Functions.

Current research on Grant NCC 1-42 involves the development of a multigroup method for the calculation of low energy evaporation neutron fluences associated with the Boltzmann equation. This research will enable one to predict radiation exposure under a variety of circumstances. Knowledge of radiation exposure in a free-space environment is a necessity for space travel, high altitude space planes and satellite design. This is because certain radiation environments can cause damage to biological and electronic systems involving both short term and long term effects.

By having apriori knowledge of the environment one can use prediction techniques to estimate radiation damage to such systems. Appropriate shielding can be designed to protect both humans and electronic systems that are exposed to a known radiation environment. This is the goal of the current research efforts involving the multi-group method and the Green's function approach.

Reference [1] presents a short history of the study of the propogation of space radiation through matter, the development of space-radiation physics and protection techniques. This reference outlines major radiation studies and their results. The accurate prediction techniques for dose fields requires either Monte Carlo type solutions, which require a great amount of computational time, or a study of the Boltzmann equation under various cir-

1

cumstances. The Boltzmann equation does not lend itself readily to analytical solutions and so various types of numerical solutions have been developed. One such numerical solution is the HZETRN code developed by Wilson et.al., reference [1]. This code has the ability to predict dose fields in simulated tissue behind a shield for high charge and high energy particles. Flux predicitions by HZETRN are based upon a straight-ahead transport of evaporation neutrons with one dimensional angular transport. In this research we investigate the transport of evaporation neutrons through a shield-target environment based upon source terms generated by the HZETRN code.

Formulation of Transport Equations

We define the differential operator

$$
\begin{aligned}
B[\phi] &= \left[\frac{\partial}{\partial x} - \frac{\partial}{\partial E} S_j(E) + \sigma_j(E) \right] \phi(x, E) \\
&= \frac{\partial \phi(x, E)}{\partial x} - \frac{\partial}{\partial E} \left[S_j(E)\phi(x, E) \right] + \sigma_j(E)\, \phi(x, E)
\end{aligned}
\tag{1}
$$

and consider the Boltzmann equation from reference [1]

$$
B[\phi_j] = \sum_k \int_0^\infty f_{jk}(E, E')\phi_k(x, E')\, dE'
\tag{2}
$$

where ϕ_j is the differential flux spectrum for the type j particles ($j = n$ neutrons or $j = p$ protons), $S_j(E)$ is the stopping power of the type j particles and $\sigma_j(E)$ is the total cross section. The term $f_{jk}(E, E')$ is a macroscopic differential energy cross section for redistribution of particle type and energy. We write

$$
f_{jk}(E, E') = \sum_\beta \rho_\beta \sigma_\beta(E') f_{jk,\beta}(E, E')
$$

where $f_{jk,\beta}(E, E')$ is an elastic collision term, σ_β is a microscopic cross section and ρ_β is the number density of β type atoms per unit mass. The collision terms are expressed as

$$
f_{jk,\beta} = f^e_{jk,\beta} + f^d_{jk,\beta}
$$

where $f^e_{jk,\beta}$ represents evaporation terms and $f^d_{jk,\beta}$ represents direct cascading terms. The evaporation process dominates over the low energies ($E < 25\,\mathrm{Mev}$) and the direct cascading effect dominates over the high energy range ($E > 25\,\mathrm{Mev}$). The equation (2) is written as

$$
B[\phi_j] = \sum_k \int_0^\infty \sum_\beta \rho_\beta \sigma_\beta(E')(f^e_{jk,\beta} + f^d_{jk,\beta})\phi_k(x, E')\, dE'.
\tag{3}
$$

2

For $j = n$ we write equation (3) in the operator form

$$B[\phi] = I_e[\phi] + I_d[\phi] + I_e[\phi_p] + I_d[\phi_p] \tag{4}$$

where $\phi = \phi_n$ and I_e, I_d are integral operators. Let ϕ_d denote the solution to the transport equation

$$B[\phi_d] = I_d[\phi_d] + I_d[\phi_p] \tag{5}$$

which is valid over all energy ranges. The solution to equation (4) is then $\phi = \phi_e + \phi_d$ where ϕ_e is the neutron flux due to evaporation and ϕ_d represents neutron flux due to direct cascading effects. The equation (4) can be expressed in the form

$$B[\phi_e] + B[\phi_d] = I_e[\phi_e] + I_e[\phi_d] + I_d[\phi_e] + I_d[\phi_d] + I_d[\phi_p] + I_e[\phi_p]. \tag{6}$$

Using the assumption that the numerical solution to equation (5) is readily obtainable from the the HZETRN code, reference [6], and that $I_d[\phi_e] \approx 0$, the equation (6) reduces to

$$B[\phi_e] = I_e[\phi_e] + I_e[\phi_d] + I_e[\phi_p] \tag{7}$$

The stopping power $S_j(E) = 0$ for neutrons and so the equation (7) reduces to the integro-differential transport equation with source term

$$\left[\frac{\partial}{\partial x} + \sigma(E)\right] \phi_e(x, E) = \sum_{\beta} \int_E^{E/\alpha_\beta} f_{s,\beta}(E, E')\phi_e(x, E') \, dE' + g(E, x) \tag{8}$$

which represents the steady state low energy neutron fluence $\phi_e(x, E)$ at depth x and energy E. The various terms in equation (8) are energy E with units of (Mev), depth in medium is x with units of (g/cm^2), $\phi_e(x, E)$ (#particles/cm^2 − Mev) is the fluence and $g(E, x) = I_e[\phi_d] + I_e[\phi_p]$ (#particles/g − Mev) is a source term. In addition, the equation (8) contains the scattering terms

$$f_{s,\beta} = \rho_\beta \sigma_\beta(E') f^e_{jk,\beta}(E, E')$$

with units of cm^2/g − Mev. The limits of integration $(E, E/\alpha_\beta)$ represent cut off values for neutron production because secondary neutrons produced have approximately the same energy as the projectile primary neutrons. The term α_β is defined as the ratio

$$\alpha_\beta = \left(\frac{A_{T_\beta} - 1}{A_{T_\beta} + 1}\right)^2 \tag{9}$$

3

and is a constant less than 1, where A_{T_i} is the atomic weight of the ith type of atom being bombarded. The quantity σ has units of (cm^2/g) is a macroscopic cross section given by

$$\sigma = \sum_j \rho_j \sigma_j \qquad (10)$$

where ρ_j is the number of atoms per gram and σ_j is a microscopic cross section in units of cm^2/atom. The reference [2] provides approximate Maxwellian averages of cross section values in barns. These values are listed in Table 1 along with other parameters of interest for selected elements.

Other units for equation (8) are obtained from the previous units by using the scale factor representing the density of the the material in units of g/cm^3.

Table 1. Parameter Values for Selected Elements					
Element	Symbol	A_{T_i}	Cross Section barns*	Density g/cm^3	α
Lithium	Li	7	1.050	.534	.563
Carbon	C	12	4.739	3.52	.716
Aluminium	Al	27	1.348	2.7	.862
Calcium	Ca	40	2.99	1.54	.905
Iron	Fe	56	11.40	7.85	.931
Lead	Pb	207	11.194	11.342	.981
* Maxwellian averages (elastic)					

Mean Value Theorem

Through out the following discussions we employ the following mean value theorem for integrals.

$Mean Value Theorem.$ For $\phi(x), f(x)$ continuous over an interval $a \le x \le b$ such that (i) $\phi(x)$ does not change sign over the interval (a,b), (ii) $\phi(x)$ is integrable over the interval (a,b), and (iii) $f(x)$ is bounded over the interval (a,b), then there exists at least one point ξ such that

$$\int_a^b f(x)\phi(x)\,dx = f(\xi) \int_a^b \phi(x)\,dx \qquad a \le \xi \le b$$

4

Multi-group method

We consider the case $\beta = 1$ which represents neutron penetration into a single element and let $\phi_e = \phi$. We integrate the equation (8) from E_i to E_{i+1} with respect to the energy E to obtain

$$\int_{E_i}^{E_{i+1}} \frac{\partial \phi(x, E)}{\partial x} \, dE + \int_{E_i}^{E_{i+1}} \sigma(E) \phi(x, E) \, dE = I_i + \xi_i \tag{11}$$

where

$$I_i = \int_{E_i}^{E_{i+1}} \int_{E}^{E/\alpha} f_{s,\beta}(E, E') \phi(x, E') \, dE' dE \tag{12}$$

and

$$\xi_i = \int_{E_i}^{E_{i+1}} g(E, x) \, dE. \tag{13}$$

As a first approximation test case we use the approximate source and scattering terms $g = g(E, x) = KEe^{-E/T}$, with K and T constants, and $f_{s,\beta}(E, E') = \frac{\sigma(E')\tau e^{-\tau(E'-E)}}{1 - e^{(1-\alpha)\tau E'}}$ so that the equation (13) is easily integrated to obtain

$$\xi_i = KT \left(E_i e^{-E_i/T} - E_{i+1} e^{-E_{i+1}/T} \right) + KT^2 \left(e^{-E_i/T} - e^{-E_{i+1}/T} \right). \tag{14}$$

We define the quantity

$$\Phi_i(x) = \int_{E_i}^{E_{i+1}} \phi(x, E) \, dE \tag{15}$$

and write the equation (11) in terms of the $\Phi_i(x)$ terms as follows. In the first term in equation (11), we interchange the order of integration and differentiation to obtain

$$\int_{E_i}^{E_{i+1}} \frac{\partial \phi(x, E)}{\partial x} \, dE = \frac{d\Phi_i(x)}{dx} \tag{16}$$

Using one of the several mean value theorems for integrals, the second term in equation (11) can be expressed as

$$\int_{E_i}^{E_{i+1}} \sigma \phi(x, E) \, dE = \overline{\sigma} \, \Phi_i(x) \tag{17}$$

where $\overline{\sigma} = \sigma(E_i + \theta(E_{i+1} - E_i))$, for some value of θ between 0 and 1.

For the term I_i in equation (12) we interchange the order of integration as illustrated in the figures 1(a)(b). The integration of equation (12) depends upon the energy partition selected. For example, the figure 1(b) illustrates an energy partition where $E_{i+1} < E_i/\alpha$ and in this case we can write the equation (12) as

5

$$I_i = \int_{E'=E_i}^{E_{i+1}} \int_{E=E_i}^{E'} H \, dEdE' + \int_{E'=E_{i+1}}^{E_i/\alpha} \int_{E=E_i}^{E_{i+1}} H \, dEdE' + \int_{E'=E_i/\alpha}^{E_{i+1}/\alpha} \int_{E=\alpha E'}^{E_{i+1}} H \, dEdE', \qquad (18)$$

where $H = f_s(E, E')\phi(x, E')$. The figure 1(c) depicts the case where $E_{i+1} = E_i/\alpha$ exactly for all i. In this special case the equation (12) reduces to

$$I_i = \int_{E'=E_i}^{E_{i+1}} \int_{E=E_i}^{E'} H \, dEdE' + \int_{E'=E_{i+1}}^{E_{i+1}/\alpha} \int_{E=\alpha E'}^{E_{i+1}} H \, dEdE'. \qquad (19)$$

The integrand H can be integrated with respect to E and the results expressed in terms of the quantities

$$F(b, a) = \int_a^b \tau e^{\tau E} \, dE = e^{\tau b} - e^{\tau a}$$

and $\qquad G(E') = \dfrac{\sigma(E')e^{-\tau E'}}{1 - e^{-(1-\alpha)\tau E'}}$

and we can write equation (19) in the form

$$\begin{aligned}
I_i &= \int_{E'=E_i}^{E_{i+1}} G(E')F(E', E_i)\phi(x, E') \, dE' \\
&+ \int_{E'=E_{i+1}}^{E_{i+1}/\alpha} G(E')F(E_{i+1}, \alpha E')\phi(x, E') \, dE'.
\end{aligned} \qquad (20)$$

To illustrate the basic idea behind the multigroup method we use one of the many mean value theorems for integrals and write the equation (20) in the form

$$I_i = G(E_i^*)F(E_i^*, E_i)\Phi_i + G(E_{i+1}^*)F(E_{i+1}, \alpha E_{i+1}^*)\Phi_{i+1}.$$

where $E_i < E_i^* < E_i/\alpha$ and $E_{i+1} < E_{i+1}^* < E_{i+1}/\alpha$. The special partitioning of the energy as illustrated in the figure 1(c) enables us to obtain from the equation (11) a system of ordinary differential equations

$$\frac{d}{dx}\begin{bmatrix} \Phi_0 \\ \Phi_1 \\ \vdots \\ \Phi_{N-2} \\ \Phi_{N-1} \end{bmatrix} = \begin{bmatrix} a_{11} & a_{12} & & & \\ & a_{22} & a_{23} & & \\ & & \ddots & \ddots & \\ & & & a_{N-1,N-1} & a_{N-1,N} \\ & & & & a_{NN} \end{bmatrix} \begin{bmatrix} \Phi_0 \\ \Phi_1 \\ \vdots \\ \Phi_{N-2} \\ \Phi_{N-1} \end{bmatrix} + \begin{bmatrix} \xi_0 \\ \xi_1 \\ \vdots \\ \xi_{N-2} \\ \xi_{N-1} \end{bmatrix} \qquad (21)$$

where $a_{i,i} = G(E_i^*)F(E_i^*, E_i) - \overline{\sigma}$ and $a_{i,i+1} = G(E_{i+1}^*)F(E_{i+1}, \alpha E_{i+1}^*)$. We further assume that for large values of N that $\Phi_i = 0$ for all $i \geq N$. This gives rise to the system of ordinary differential equations

$$\frac{d\overline{y}}{dx} = A\overline{y} + \overline{b}$$

6

subject to the initial conditions $\bar{y}(0) = \bar{0}$. Here $\bar{y}$ is the column vector $\text{col}(\Phi_0, \Phi_1, \ldots, \Phi_{N-1})$, A is an N by N upper triangular matrix and $\bar{b}$ is the column vector $\text{col}(\xi_0, \xi_1, \ldots, \xi_{N-1})$.

In a similar manner the integrals in equation (18) can be evaluated for other kinds of energy partitioning and we will obtain a system of equations having the form of equation (21). However, for these other energy partitions the structure of the N by N square matrix A will change. It remains upper triangular but with more off diagonal elements which depend upon the energy partition. For our purposes the system of equations (21) will be used to discuss some of the problems associated with the multigroup method.

We construct the energy partition

$$\left\{ E_0, E_0/\alpha, E_0/\alpha^2, \ldots, E_0/\alpha^N \right\},$$

where $E_0 = 0.1 \, \text{Mev}$, for the selected elements of lithium, aluminum, and lead. The table 2 illustrates integer values of N necessary to achieve energies greater than 30 Mev.

Table 2. Energy Partition Size N			
Element	α	N	$0.1/\alpha^N$
Lithium	0.563	10	31.53
Aluminium	0.862	39	32.75
Lead	0.981	298	30.38

For energy partitions where $E_{i+1} < E_i/\alpha$ the values of N will be larger and when $E_{i+1} > E_i/\alpha$ the values of N will be smaller. The cases where $E_{i+1} > E_i/\alpha$ give rise to situations like that illustrated in the figure 1(d). In this figure the area A_1 is associated with the integral defining Φ_i and the area A_2 is a remaining area associated with an integral which is some fraction of the integral defining Φ_{i+1} which is outside the range of integration and so some approximation must be made to define this fractional part. This type of partitioning produces errors, due to any approximations, but it has the advantage of greatly reducing the size of the N by N matrix A.

The case of neutron penetration into a composite material gives rise to the case where $\beta > 1$ in the equation (8). In this special case the equation (12) becomes

$$I_i = \sum_j \int_{E_i}^{E_{i+1}} \int_E^{E/\alpha_j} f_{s_j}(E, E') \phi(x, E') \, dE' dE.$$

We select $\alpha = \max(\alpha_1, \alpha_2, \ldots, \alpha_j)$ and construct the energy partition where $E_{i+1} = E_i/\alpha$. We then obtain a system of differential equations having the upper triangular form

$$\frac{d}{dx}\begin{bmatrix} \Phi_0 \\ \Phi_1 \\ \vdots \\ \vdots \\ \Phi_{N-1} \end{bmatrix} = \begin{bmatrix} a_{11} & a_{12} & a_{13} & \cdots & a_{1N} \\ & a_{22} & a_{23} & \cdots & a_{2N} \\ & & a_{33} & \cdots & \vdots \\ & & & \ddots & \vdots \\ & & & & a_{NN} \end{bmatrix} \begin{bmatrix} \Phi_0 \\ \Phi_1 \\ \vdots \\ \vdots \\ \Phi_{N-1} \end{bmatrix} + \begin{bmatrix} \xi_0 \\ \xi_1 \\ \vdots \\ \vdots \\ \xi_{N-1} \end{bmatrix} \qquad (22)$$

Energy Partition for Finite Values of N

Consider the case of neutron fluence in a single shield material with the energy partitioning as illustrated in the figure 1(c). This is the case where successive energy values are given by $E_{i+1} = E_i/\alpha$ for all values of the index i as i ranges from 0 to N. We select a finite value for N, say $N = 10$, and select E_0 large enough such that the assumption $\Phi_N = 0$ holds true. The system of equations (21) is then a closed system and we can solve for the terms $\{\Phi_0, \ldots, \Phi_{N-1}\}$. If we march backwards N energy partitions from the original starting value E_0, we obtain a new value for E_0, such that the final value Φ_N equals the old starting value Φ_0. The term $a_{N,N+1}\Phi_N$ in the equation (21) is now known and can be moved into the right hand side of the system along with the ξ_{N-1} term. Continuing in this manner we can define groups of energy partitions of size N, where in each group $E_{i+1} = E_i/\alpha$ are the energy values considered. The starting value E_0 changes for each group and, except for the highest energy group, we will have the value of Φ_0 from a higher group equal to the value of Φ_N from the lower energy group. The grouping scheme is illustrated in the Figure 2. In this way, we can break a large energy partitioning into groups of N equations, where the highest energy group of equations is solved first and the lowest group of equations is solved last. The nonzero elements $a_{i,j}$ for the matrix A in equation (22) consists of the diagonal elements and the first diagonal above the main diagonal. This gives the values

$$a_{ii} = G(E_i^*)F(E_i^*, E_i) - \overline{\sigma}$$

$$a_{i,i+1} = G(E_{i+1}^*)F(E_{i+1}, \alpha E_{i+1}^*)$$

for $i = 1, \ldots, N$ where E_i^* and E_{i+1}^* are selected mean values associated with the lower and upper triangles illustrated in the figure 1(c). These mean values vary with energy and were selected as

$$E_i^* = E_i + \theta_1(E_{i+1} - E_i)$$

$$E_{i+1}^* = E_{i+1} + \theta_2(E_{i+2} - E_{i+1})$$

8

where

$$\theta_1 = \begin{cases} \gamma_1 + m_{11}(E - E_{11}) - \delta_1 & E > E_{11} \\ \gamma_1 + m_{12}(E - E_{11}) - \delta_1 & E_{22} < E < E_{11} \\ \gamma_3 + m_{13}(E - E_{22}) - \delta_1 & E < E_{22} \end{cases}$$

and

$$\theta_2 = \begin{cases} \gamma_2 + m_{21}(E - E_{11}) & E > E_{11} \\ \gamma_2 + m_{22}(E - E_{11}) & E_{22} < E < E_{11} \\ \gamma_4 + m_{23}(E - E_{22}) & E < E_{22} \end{cases}$$

where

$\gamma_1 = 0.93$	$m_{11} = 0.0030485$	$m_{21} = 0.004355$
$\gamma_2 = 0.90$	$m_{12} = 0.2490258$	$m_{22} = 0.249026$
$\gamma_3 = 0.30$	$m_{13} = -0.3937186$	$m_{23} = -0.255920$
$\gamma_4 = 0.27$	$E_{11} = 3.037829$	$E_{22} = 0.5079704$

and δ_1 has the values, 0.0 for lead, 0.02 for aluminum, and 0.075 for lithium. In addition, we set $\theta_3 = \theta_1$ and $\theta_4 = \theta_2$ because of the symmetry of the triangles involved in the calculations. The above values of θ for the mean value theorems were determined by trial and error so that the multigroup curves would have the correct shape. These selections for the mean values are not unique.

Solution Method Shield Material

We consider the energy partition $E_{i+1} = E_i/\alpha$ and the resulting system of equations (21). The solution of this system of equations is obtained by first solving the last equation of the system. This equation has the form

$$\frac{d\Phi_{N-1}}{dx} = a_{NN}\Phi_{N-1} + \xi_{N-1}(x), \qquad \Phi_{N-1}(0) = 0$$

and has the solution

$$\Phi_{N-1}(x) = e^{a_{NN}x}\left(\Phi_{N-1}(0) + \int_0^x \xi_{N-1}(s)e^{-a_{NN}s}\,ds\right)$$

which implies

$$\Phi_{N-1}(x_0 + \Delta x) = e^{a_{NN}\Delta x}\Phi_{N-1}(x_0) + e^{a_{NN}(x_0+\Delta x)}\int_{x_0}^{x_0+\Delta x} \xi_{N-1}(s)e^{-a_{NN}s}\,ds.$$

We then consider each of the remaining equations above the last equation. A typical equation from this stack has the form

$$\frac{d\Phi_i}{dx} = a_{ii}\Phi_i + f_i(x), \qquad \Phi_i(0) = 0$$

9

where $f_i(x) = \xi_i(x) + a_{i,i+1}\Phi_{i+1}(x)$ is known since $\Phi_{i+1}(x)$ is calculated before $\Phi_i(x)$. This typical equation has the solution

$$\Phi_i(x) = a^{a_{ii}x}\left(\Phi_i(0) + \int_0^x f_i(s)e^{-a_{ii}s}\,ds\right)$$

which implies

$$\Phi_i(x_0 + \Delta x) = e^{a_{ii}\Delta x}\Phi_i(x_0) + e^{a_{ii}(x_0+\Delta x)}\int_{x_0}^{x_0+\Delta x} f_i(s)e^{-a_{ii}s}\,ds$$

Another Viewpoint for the Resulting System of Equations

The equations resulting from the energy partitioning of each group can be expressed as a system of ordinary differential equations

$$\frac{d\Phi_i}{dx} + \overline{\sigma}\Phi_i = I_i + \xi_i, \quad i = 1, 2, \ldots, N-1$$

which is equivalent to the vector system of ordinary differential equations

$$\frac{d\overline{y}}{dx} = A\overline{y} + \overline{b}$$

subject to the initial condition $\overline{y}(0) = \overline{0}$. Here $\overline{y}$ is the column vector $\mathrm{col}(\Phi_0, \Phi_1, \ldots, \Phi_{N-1})$, A is a N by N upper triangular matrix, and $\overline{b}$ is the column vector $\mathrm{col}(\xi_0, \xi_1, \ldots, \xi_{N-1})$ From the solution of this system of ordinary differential equations we calculate the average fluence over each energy interval

$$\Phi_{i-avg} = \frac{1}{E_{i+1} - E_i}\int_{E_i}^{E_{i+1}} \phi(x)\,dx.$$

Fundamental matrix solution

Let $Y(x) = e^{Ax}$ denote the fundamental matrix solution defined by the matrix differential equation

$$\frac{dY}{dx} = AY, \qquad Y(0) = I$$

where I is the N by N identity matrix and A is an upper triangular matrix. The solution of the system of equations (21) can then be represented in the form

$$\overline{y}(x) = Y(x)\int_0^x Y^{-1}(s)\overline{b}\,ds = \int_0^x Y(x-s)\overline{b}\,ds \tag{23}$$

10

The exponential matrix $Y(x)$ satisfies the properties that

$$AY(x) = Y(x)A$$
$$Y(-x) = Y^{-1}(x) \tag{24}$$
$$\text{and} \quad Y(x+s) = Y(x)Y(s)$$

Consequently, for $\bar{b}$ constant, the solution given by equation (24) can be represented in the form

$$\bar{y}(x) = (Y(x) - I)A^{-1}\bar{b}. \tag{25}$$

The solution, as given by equation (25) can also be expressed in terms of a Green's function for discrete systems. We rewrite the solution system (25) in the equivalent form

$$\bar{y}(x+h) = (Y(x+h) - I)A^{-1}\bar{b}$$
$$\bar{y}(x+h) = (Y(x)Y(h) - I)A^{-1}\bar{b}$$
$$\bar{y}(x+h) = Y(h)(Y(x) - Y(-h) + I - I)A^{-1}\bar{b} \tag{26}$$
$$\bar{y}(x+h) = Y(h)\bar{y}(x) + (Y(h) - I)A^{-1}\bar{b}.$$

If $\bar{b}$ is not constant, but a function of x, then the solution is left in the integral form of equation (23) and becomes

$$\bar{y}(x) = Y(x) \int_0^x Y^{-1}(\xi)\bar{b}(\xi)\,d\xi.$$

In this case, we have

$$\bar{y}(x+h) = Y(x+h)\int_0^{x+h} Y^{-1}(s)\bar{b}(s)\,ds = Y(h)\bar{y}(x) + Y(x)Y(h)\int_x^{x+h} Y^{-1}(s)\bar{b}(s)\,ds.$$

Calculation of the Exponential Matrix Exp(Ax)

The fundamental matrix solution $Y(x) = e^{Ax}$ can be calculated from the Putzer algorithm, reference [3]. This algorithm states that for A an $n \times n$ matrix with eigenvalues $\lambda_1, \lambda_2, \ldots \lambda_n$, the exponential matrix is given by

$$e^{Ax} = \sum_{j=0}^{n-1} r_{j+1}(x)P_j$$

where

$$P_0 = I, \qquad P_j = \Pi_{k=1}^j (A - \lambda_k I), \qquad j = 1, \ldots, n$$

11

and $r_1(x), \ldots, r_n(x)$ are solutions of the triangular system

$$\frac{dr_1}{dx} = \lambda_1 \, r_1 \qquad r_1(0) = 1$$

$$\frac{dr_j}{dx} = r_{j-1}(x) + \lambda_j \, r_j(x), \qquad r_j(0) = 0$$

for $j = 2, \ldots, n$. Here each eigenvalue is listed in an ordered form from high to low values and multiplicity of eigenvalues is permissible.

Numerical Solution

The solutions obtain from the system of equations (21) or (22) depend upon the selection of mean values associated with each energy interval. The selection of these mean values is determined by examing the numerical solution in certain special cases. We obtain a numerical solution of equation (8) in the special case given by $g = g(E, x) = K E e^{-E/T}$ where K (#particles/cm^3 Mev) and T (Mev), are constants. We construct the solution over the spatial domain $x \geq 0$ and energy range $.1 \leq E \leq 80$ Mev. This domain is discretized by constructing a set of grid points $x_i = i\Delta x$ and $E_j = j\Delta E$ for some grid spacing defined by Δx and ΔE values. For i, j integers we define $u_{i,j} = \phi(x_i, E_j)$, then the transport differential-integral equation (8) can be written in a discrete form. We use the starting values $u_{0,j} = 0$ and $v_{0,j} = 0$. For the first step in Δx we write

$$u_{1,j} = \Delta x K E_j e^{-E_j/T}. \tag{27}$$

followed by the numerical calculation of

$$v_{i,j} = \int_{E_j}^{E_j/\alpha} \frac{\sigma(E')\tau e^{-\tau(E'-E_j)}}{1 - e^{-(1-\alpha)\tau E'}} u(x_i, E') \, dE', \tag{28}$$

when $i = 1$. After each numerical step the integrals of the type $v_{i,j}$ given by equation (29) are evaluated using Simpson's 1/3 rule. We evaluate the equation (28) for $j = 0, 1, \ldots$, we then use a two step algorithm in a repetitive fashion to advance the solution. For values of α near one the numerical solution of equation (8) requires that ΔE become small. For numerical accuracy we must have $\Delta x << \Delta E$. The low energy spectrum then becomes difficult to calculate without special procedures, reference [1]. In this case we use a two step modified Euler predictor-corrector scheme, references [4],[5], which is defined by

$$\text{Second step:} \quad f_{1,j} = v_{1,j} + E_j e^{-E_j} - \sigma u_{1,j}$$

$$u_{2,j} = \begin{cases} u_{1,j} + \Delta x \, f_{1,j} & j = 0 \\ \frac{1}{2}(u_{1,j-1} + u_{1,j+1}) + \Delta x \, f_{1,j} & j > 0 \end{cases} \tag{29}$$

$$\text{Third step:} \quad f_{2,j} = v_{2,j} + E_j e^{-E_j} - \sigma u_{2,j}$$

$$u_{3,j} = u_{1,j} + 2\Delta x \, f_{2,j}$$

12

The second step is an adaption of the Fredrichs method from reference [4]. The third step is a central difference second order step in Δx. After each 100 such applications of the above numerical two step algorithm, we apply the following stability correction as suggested in reference [5].

$$f_{3,j} = v_{3,j} + E_j e^{-E_j} - \sigma\, u_{3,j}$$
$$u_{3,j} = \frac{1}{2}\left(u_{3,j} + u_{2,j}\right) + \Delta x\, f_{3,j} \tag{30}$$

Recurrsive Solution

In the special case g(E,x)=g(E), we assume a solution to equation (8) of the form

$$\phi(x,E) = \sum_{n=1}^{\infty} \phi_n(E) f_n(x) = \phi_1(E) f_1(x) + \phi_2(E) f_2(x) + \cdots \tag{31}$$

We substitute this series into the equation (8) and obtain a solution by requiring that

$$\phi_1(E) = g(E) \qquad\qquad\qquad f_1'(x) + \sigma f_1(x) = 1$$
$$\phi_{n+1}(E) = \int_E^{E/\alpha} f_s(E,E')\phi_n(E')\,dE' \quad n = 1,2,3,\ldots \qquad f_n'(x) + \sigma f_n(x) = f_{n-1}(x) \tag{32}$$

where the differential equations are subject to the initial condition that $f_n(0) = 0$ for all n. Here the $\phi_n(E)$ terms are defined recurrsively and take a great deal of computational time for large values of n. The differential equations have the solutions given by the recurrsive relations

$$f_1(x) = \frac{1}{\sigma}\left(1 - e^{-\sigma x}\right)$$
$$f_n(x) = \int_0^x f_{n-1}(u) e^{-\sigma(x-u)}\,du \tag{33}$$

which are easily evaluated for as large an n as desired. We find numerically that $|f_n(x)|$ decreases with increasing n when x is less than 1 and increases for $x > 1$ so that the series solution does not converge in this case. For $|x|$ less than or equal to one we calculate the solution given by equation (33) for terms through $n = 5$ and $n = 6$ and compared them with the numerical solution. The mean values associated with the numerical solution of equations (21) and (22) where then adjusted in order that all solutions agree for this special circumstance. We then used these same mean values which where associated with numerical source terms as provided by the HZETRN code.

Comparison of Multigroup and Other Solutions

The numerical solutions and recurrsive solutions are compared with the multigroup solution for neutron penetration in lithium, aluminum and lead mediums for the case

$n = 2$. The results are illustrated in the figures 3,4, and 5. Excellent agreement is obtain in these cases. In these figures, the solid line represents the numerical solution. The circles represent the recursive solution and the triangles represent the multigroup solution. The various curves were calculated for depths of $x = 0.1, 0.5, 1.0, 5.0, 10.0, 50.0$ and 100.0 centimeters. Similarly, the figures 6,7 and 8 illustrate the multigroup method in the case $n = 10$ for neutron penetration into lithium, aluminium and lead respectively.

The multigroup method has a huge advantage in the computational time needed to calculate the solution. The multigroup method takes less than one minute of computational time while the other methods require many hours of computational time.

Application for $Al - H_2O$ shield-target configuration.

We now apply our previous development to an application of the multigroup method associated with an aluminium-water shield-target configuration. In particular, we consider the case where the source term $g(E, x)$, in equation (8), represents evaporation neutrons produced per unit mass per Mev and is specified as a numerical array of values corresponding to various shield-target thicknesses and energies. The numerical array of values is produced by the radiation code HZEBIO, which is a modification of the radiation code HZETRN developed by Wilson, et. al., reference [6]. The numerical array of values are actually given in the form $g(E_i, x_j, y_k)$ in units of particles/$gm - Mev$, where y_k represents discrete values for various target thicknesses of water in gm/cm^2, x_j represents discrete values for various shield thicknesses of aluminium, also in units of gm/cm^2, and E_i represents discrete energy values in units of (Mev). We use these discrete source term values in the following way. We consider first the solution of equation (8) solved by the multigroup method with no target material i.e. all shield material with target thickness $y = 0$. We next consider the cases 2,3,... of discrete shield thickness $x_2, x_3, ...$ and apply the multigroup method to the solution of equation (8) applied to all target material $y > 0$. For each x_i-value considered, the initial conditions are obtained from the previous solutions generated where $y = 0$. This represents the application of the multigroup method to two different regions. Region 1 of all shield material and region 2 of all target material. We then continue to apply the multigroup method to region 2 for each discrete value of shield thickness, where the initial conditions on the start of the second region represents exit conditions from the shield region 1. This provides for continuity of the solutions for the fluence between the two regions. In this way we develop a series of graphs for fluence vs energy associated with various shield thickness.

14

In our application of the multigroup method we consider the case where the source term $g(E,x)$, the scattering term $f_s(E,E')$ and cross section $\sigma(E)$ are all given numerically (obtained from the above HZETRN code).

For a single shield material we solve

$$\left[\frac{\partial}{\partial x} + \sigma(E)\right]\phi(x,E) = \int_E^{E/\alpha_1} f_{s_1}(E,E')\phi(x,E')\,dE' + g(E,x) \tag{34}$$

Integration of equation (34) from E_i to E_{i+1} produces

$$\begin{aligned}
\int_{E_i}^{E_{i+1}} \frac{\partial\phi}{\partial x}\,dE + \int_{E_i}^{E_{i+1}} \sigma(E)\phi(x,E)\,dE = \\
\int_{E_i}^{E_{i+1}} \int_E^{E/\alpha_1} f_{s_1}(E,E')\phi(x,E')\,dE'dE + \int_{E_i}^{E_{i+1}} g(E,x)\,dE
\end{aligned} \tag{35}$$

We define the quantities

$$\Phi_i = \int_{E_i}^{E_{i+1}} \phi(x,E)\,dE \qquad b_i = \int_{E_i}^{E_{i+1}} g(E,x)\,dE \tag{36}$$

and interchange the order of integration of the double integral terms in equation (36). We then apply a mean value theorem to obtain the result

$$\begin{aligned}
\frac{d\Phi_i}{dx} + \overline{\sigma}\,\Phi_i = \int_{E_i}^{E_{i+1}} \int_{E=E_i}^{E'} f_{s_1}(E,E')\,dE\,\phi(x,E')\,dE' + \\
\int_{E_{i+1}}^{E_{i+2}} \int_{E=\alpha_1 E'}^{E_{i+1}} f_{s_1}(E,E')\,dE\,\phi(x,E')\,dE' + b_i
\end{aligned} \tag{37}$$

where $E_i < E' < E_{i+1}$. The first double integral in equation (37) represents integration over the lower triangle illustrated in the figure 1(c). The second double integral in equation (38) represents integration over the upper triangle illustrated in the figure 1(c). Let

$$g_1(E') = \int_{E=E_i}^{E'} f_{s_1}(E,E')\,dE \quad \text{and} \quad g_2(E') = \int_{E=\alpha_1 E'}^{E_{i+1}} f_{s_1}(E,E')\,dE \tag{38}$$

then employ another application of a mean value theorem for integrals to write equation (37) in the form

$$\frac{d\Phi_i}{dx} + \overline{\sigma}\,\Phi_i = g_1(E_i + \theta_1(E_{i+1}-E_i))\Phi_i + g_2(E_{i+1}+\theta_2(E_{i+2}-E_{i+1}))\Phi_{i+1} + b_i \tag{39}$$

This produces the coefficients associated with the energy interval E_i to E_{i+1} given by

$$a_{ii} = g_1 - \overline{\sigma} \qquad \text{and} \qquad a_{i,i+1} = g_2 \tag{40}$$

needed for the numerical integration of equations (21). In this way the diagonal and off diagonal elements of the coefficient matrix in equation (21) are calculated.

For a compound target material, comprised of material 1 and material 2, there are two values for α. A value α_1 is selected for material 1 and a value α_2 is selected for the material 2 of the compound material. In this case the equation (34) takes on the form

$$
\begin{aligned}
\left[\frac{\partial}{\partial x} + \sigma(E) \right] \phi(x, E) = & \\
\int_E^{E/\alpha_1} f_{s_1}(E, E') \phi(x, E') \, dE' + & \\
\int_E^{E/\alpha_2} f_{s_2}(E, E') \phi(x, E') \, dE' + g(E, x) &
\end{aligned}
\tag{41}
$$

where f_{s_1} and f_{s_2} are scattering terms associated with the respective materials. These terms are calculated in the HZETRN code. We consider two cases. The first case requires that the E/α_2 line be above the E/α_1 line.(See figure 1(d)) The second case is where $\alpha_2 = 0$ (the hydrogen case), and the limits of integration for the second integral go to infinity. We consider each case separately.

For the first case we assume that $\alpha_1 > \alpha_2 > 0$ and we select the exact energy spacing dictated by the E/α_2 line. We then proceed as we did using the single shield material. We integrate equation (41) from E_i to E_{i+1} and interchange the order of integration on the double integral terms. Define $b_i = \int_{E_i}^{E_{i+1}} g(E, x) \, dE$ and obtain the equations

$$\frac{d\Phi_i}{dx} + \overline{\sigma} \Phi_i = I_{11} + I_{12} + I_{21} + I_{22} + b_i \tag{42}$$

where now the I_{21} and I_{22} integrals have, because of the exact spacings, the forms

$$
\begin{aligned}
I_{21} &= \int_{E_i}^{E_{i+1}} \int_{E=E_i}^{E'} f_{s_2}(E, E') \, dE \, \phi(x, E') \, dE' \\
I_{22} &= \int_{E_{i+1}}^{E_{i+2}} \int_{E=\alpha_2 E'}^{E_{i+1}} f_{s_2}(E, E') \, dE \, \phi(x, E') \, dE'
\end{aligned}
\tag{43}
$$

Defining the terms

$$h_{1(i)}(E') = \int_{E=E_i}^{E'} f_{s_i}(E, E') \, dE, \quad i = 1, 2$$

$$h_{2(i)}(E') = \int_{E=\alpha_2 E'}^{E_{i+1}} f_{s_i}(E, E') \, dE \quad i = 1, 2$$

16

and using the mean value theorem for integrals we obtain

$$I_{21} = h_{1(2)}(E_i + \theta_1(E_{i+1} - E_i))\Phi_i \quad \text{and} \quad I_{22} = h_{2(2)}(E_{i+1} + \theta_2(E_{i+2} - E_{i+1}))\Phi_{i+1}$$

where θ_1 and θ_2 define intermediate energy values associated with the mean value theorem. The integrals I_{11} and I_{12} are associated with integration limits $(E, E/\alpha_1)$ and energy intervals dictated by our selection of α_2 for determining the exact energy spacings. These integrals are associated with the trapezoidal area 1 and triangular area 2 illustrated in the figure 1(d). These areas are a fraction of the triangle area's associated with the line $E' = E/\alpha_2$. These fractions are given by

$$
\begin{aligned}
f_1 &= \frac{\frac{1}{2}(E_{i+1} - E_i)^2 - \frac{1}{2}(E_{i+1} - E_i/\alpha_1)(E_{i+1} - \alpha_1 E_{i+1})}{\frac{1}{2}(E_{i+1} - E_i)(E_{i+2} - E_{i+1})} \\
f_2 &= \frac{(E_{i+1}/\alpha_1 - E_{i+1})(E_{i+1} - \alpha_1 E_{i+1})}{(E_{i+1} - E_i)(E_{i+2} - E_{i+1}))}
\end{aligned}
\tag{44}
$$

and we write

$$I_{11} = f_1 h_{1(1)}\Phi_i \quad \text{and} \quad I_{12} = f_2 h_{2(1)}\Phi_{i+1} \tag{45}$$

The coefficients for our system of differential equations (22) are then given by

$$
\begin{aligned}
a_{11} &= h_{1(2)} + f_1 h_{1(1)} - \overline{\sigma} \\
a_{12} &= h_{2(2)} + f_2 h_{2(1)}.
\end{aligned}
\tag{46}
$$

For the case 2, of hydrogen, $\alpha_2 = 0$ and so one of the limits of integration becomes infinite. We let α_1 determine the energy spacing in this case. We again integrate equation (42) over and energy interval (E_i, E_{i+1}) which is determined by the $E' = E/\alpha_1$ line. Using the definitions given by equations (36) we integrate the equations (41) over the interval (E_i, E_{i+1}) and then interchange the order of integration in the resulting double integrals to obtain

$$\frac{d\Phi_i}{dx} + \overline{\sigma}\Phi_i = I_1^* + I_2^* + b_i$$

where

$$I_1^* = \int_{E_i}^{E_{i+1}} \int_{E=E_i}^{E'} f_{s_1}(E, E')\, dE\, \phi(x, E')\, dE' + \int_{E_{i+1}}^{E_{i+2}} \int_{E=\alpha_1 E'}^{E_{i+1}} f_{s_1}(E, E')\, dE\, \phi(x, E')\, dE'$$

and

$$I_2^* = \int_{E_i}^{E_{i+1}} \int_{E_i}^{E'} f_{s_2}(E, E')\, dE\, \phi(x, E')\, dE' + \sum_{j=1}^{N} \int_{E_{i+j}}^{E_{i+j+1}} \int_{E_i}^{E_{i+1}} f_{s_2}(E, E')\, dE\, \phi(x, E')\, dE'$$

17

where for all N^* greater than some integer $N > 0$ we know that $f_{s_2}(E, E')$ will be zero. We define

$$h_3(E') = \int_{E_i}^{E'} f_{s_1}(E, E')\, dE, \quad E_i < E' < E_{i+1}$$

$$h_4(E') = \int_{\alpha_1 E'}^{E_{i+1}} f_{s_1}(E, E')\, dE, \quad E_{i+1} < E' < E_{i+2}$$

$$h_5(E') = \int_{E_i}^{E'} f_{s_2}(E, E')\, dE, \quad E_i < E' < E_{i+1}$$

$$h_{6(j)} = \int_{E_{i+j}}^{E_{i+j+1}} f_{s_2}(E, E')\, dE, \quad E_{i+j} < E'_j < E_{i+j+1}$$

then we can write the coefficients associated with the system of differential equations as

$$a_{i,i} = h_3 + h_5 - \overline{\sigma} \qquad a_{i,i+3} = h_{6(3)}$$

$$a_{i,i+1} = h_4 + h_{6(1)} \qquad\qquad \vdots$$

$$a_{i,i+2} = h_{6(2)} \qquad a_{i,i+n} = h_{6(n)}$$

In this way we generate a system of equations having the triangular form given by the equations (22).

Various comparisons have been made to check the validity of the multigroup method. The figure 9 shows low energy neutron fluence vs depth for a shield-target aluminium water medium. Note the increase in low energy neutron production at the aluminium water interface at a depth of $100 g/cm^2$. This is due to high energy neutrons colliding with hydrogen atoms. In these type of collisions the high energy neutrons give up over one-half of their energy, thus increasing the low energy neutron fluence.

Using the source terms generated by the HZETRN program for an aluminium water configuration the figures 10 through 19 result for the evaporation neutron fluence as a function of energy for various shield thicknesses. The shield thicknesses in these figures are $y = 0.0, 0.3, 1.0, 5.0, 10.0, 20.0, 30.0, 50.0$, and 100.0 g/cm^2. The figures 20,21 and 22 illustrate the comparison of the old HZETRN code results with and without the addition of the evaporation neutrons. These results are also compared with the Monte Carlo results for fluence associated with the February 1956 solar flare data. The multigroup method for the calculation of the low energy evaporation neutrons is computed much faster numerically than any of the previous approximation methods. The method also produced much more accurate results when compared to the Monte Carlo method, see for example reference [157] and [158] of Appendix A.

REFERENCES

[1] John W. Wilson, L.W. Townsend, W. Schimmerling, G.S. Khandelwal, F.Kahn, J.E. Nealy, F.A. Cucinotta, L.C. Sinonsen, J.L. Shinn, J.W. Norbury, **Transport Methods and Interactions for Space Radiations**, NASA Publication 1257, December 1991.

[2] B.A. Magurno, R.R. Kinsey, F.M. Scheffel, **Guidebook for the ENDF/B-V Nuclear Data Files**, NP-2510, Research Project 975-1, BNL-NCS-31451,ENDF-328, Brookhaven National Laboratory, July 1982.

[3] P. Waltham, **A Second Course in Elementary Differential Equations**, Academic Press, 1986.

[4] C.A.Hall, T.A. Porsching, **Numerical Analysis of Partial Differential Equations**, Prentice Hall, 1990.

[5] Germund Dahlquist, Åke Björck, **Numerical Methods**, Prentice Hall, 1974.

[6] J.W. Wilson, F.F. Badavi, F.A. Cucinotta, J.L. Shinn, G.D. Badhwar, R. Silberberg, C.H. Tsao, L.W. Townsend, R.K. Tripathi, **HZETRN: Description of a Free-Space Ion and Nucleon Transport and Shielding Computer Program**, NASA Technical Paper 3495, May 1995.

APPENDIX A

Publications that have resulted from research associated
with grant NCC 1-42.

1. J.W. Wilson and G.S. Khandelwal, "Response of Large Cavity Ion Chambers of Space Protons," Nuclear Technology Journal 52 , 120-123 (1981).

2. J.W. Wilson and L.W. Townsend, "An Optical Model for Composite Nuclear Scattering," Canadian J. Phys. 59 , 1569-1576 (1981).

3. G.S. Khandelwal, "Stopping Power of K and L Electrons," Phys. Rev. A 5, 2923-2985 (1982).

4. E. Kamaratos, C.K. Chang, J.W. Wilson and Y.J. Xu, " Valence Bond Effects on Mean Excitation Energies for Stopping Power in Metals," Phys. Lett. 92A, 363-365 (1982).

5. J.W. Wilson, C.K. Chang, Y. J. Xu and E. Kamaratos, " Ionic Bond Effects on the Mean Excitation Energy for stopping Power," J. Appl. Phys. 53, 828-830 (1982).

6. J.W. Wilson, and Y.J. Xu, " Metallic Bond Effects on Mean Excitation Energies for Stopping Powers," Phys. Lett. 90A, 253-255 (1982).

7. H.B. Bidasaria and L.W. Townsend, "Phenomenological Harmonic Well Optical Potential Analysis of Proton-Carbon Elastic Scattering," Bull. Am. Phys. Soc. 27, 509 (1982).

8. L.W. Townsend and H.B. Bidasaria, "An Optical Potential Description of Heavy Ion Collisions Below 200 MeV/Nucleon," Bull. Am. Phys. Soc. 27, 549 (1982).

9. L.W. Townsend, J.W. Wilson and H.A. Bidasaria, "On the Geometric Nature of High-Energy Nucleus-Nucleus Reaction Cross Sections," Canadian J. Phys. 60, 1514-1518 (1982).

10. H.B. Bidasaria and L.W. Townsend, "Analytical Optical Potentials for Nucleon-Nucleus and Nucleus-Nucleus Collisions Involving Light and Medium Nuclei," NASA TM-83224 (1982).

11. H.B. Bidasaria and L.W. Townsend, "Phenomenological Optical Potential Analysis of Proton-Carbon Elastic Scattering at 200 Mev," NASA TM-84498 (1982).

20

12. L.W. Townsend and H.B. Bidasaria, "Improvements to the Langley HZE Abrasion Model," NASA TM-84542 (1982).

13. J.W. Wilson, G.M. Walker, R.A. Outlaw and L.V. Stock, "A Model for Proton-Irradiated GaAs Solar Cells," IEEE Photovoltaic Specialist Conference, San Diego, California, September 27-30, 1982.

14. Preliminary Analysis of Accelerated Space Flight Ionizing Radiation Testing, NASA TM-83209 (1982).

15. H.B. Bidasaria, L.W. Townsend and H.B. Bidasaria, "Complex WKB Analysis of Carbon-Carbon Rainbow scattering," Bull. Am. Phys. Soc. 28, 658 (1983).

16. L.W. Townsend and H.B. Bidasaria, "Analytical Determinations of Single-Folding Optical Potentials," NASA TM-84611 (1983).

17. H.B. Bidasaria and L.W. Townsend, " Microscopic Optical Potential analyses of Carbon-Carbon Elastic Scattering," Canadian J. Phys. 61 , 1660-1662 (1983).

18. H.B. Bidasaria, L.W. Townsend and J.W. Wilson, " Theory of Carbon-Carbon Scattering from 200 to 290 MeV," J. Phys. G: Nuclear Phys. 9 , L17-L20 (1983).

19. L.W. Townsend, H.B. Bidasaria and J.W. Wilson, " Eikonal phase Shift Analyses of Carbon-Carbon Scattering," Canadian J. Phys. 61 , 867-871 (1983).

20. L.W. Townsend, J.W. Wilson and H.B. Bidasaria, " Heavy-Ion Total and Absorption Cross Sections Above 25 MeV/Nucleon," NASA TP-2138 (1983).

21. L.W. Townsend, J.W. Wilson and H.B. Bidasaria, " Nucleon and Deutron Scattering Cross Sections From 25 MeV/Nucleon to 22.5 GeV/Nucleon," NASA TM-84636 (1983).

22. L.W. Townsend, H.B. Bidasaria and J.W. Wilson, "Complex WKB Solutions for B2C + B2C Scattering," Proceedings of the 6th High-Energy Heavy Ion Study and 2nd Workshop on Anomalons, Berkley, CA, pp151-154, LBL Report LBL-16281 (1983).

23. L.W. Townsend, J.W. Wilson and H.B. Bidasaria, " Neon Transport in Selected Organic Composites," NASA TM-85693 (1984).

24. J.W. Wilson, Y.J. Xu, E. Kamaratos and C.K. Chang, "Mean Excitation Energies for Stopping Powers in Various Materials using Local Plasma Oscillator Strengths," NASA TP-2271 (1984).

25. Equivalent Electron Fluence for Space Qualification of Shallow Junction Heteroface GaAs Solar Cells, IEEE Transactions on Electron Devices, 31, 622-625 (1984).

26. J.W. Norbury, L.W. Townsend and J.W. Wilson, " Fragmentation of Relativistic 16O Projectiles by 9Be and 208Pb Target Nuclei," Bull. Am. Phy. Soc. 29, 687 (1984).

27. J.W. Wilson and F.A. Cucunotta, "Dose in Critical Body Organs in Low Earth Orbits," NASA TM-85778 (1984). 33 pages.

28. Atomic Mean Excitation Energies for Stopping Powers from Local Plasma Oscillator Strengths, J. Applied Physics 56, 860-863 (1984).

29. J.W. Norbury, P.A. Deutchman and L.W. Townsend, "A particle-Hole Formalism for Pion Production from Isobar Formation and Decay in Peripheral Heavy Ion Collisions," Bull. Am. Phys. Soc. 29 , 688 (1984).

30. Y.J. Xu, G.S. Khandelwal and J.W. Wilson, "Intermediate Energy Proton Stopping Power for Hydrogen Molecules and Monoatomic Helium Gas," Phys. Lett. A 100A, 137-140 (1984).

31. Y.J. Xu, G.S. Khandelwal and J.W. Wilson, "Low Energy Proton Stopping Power of N2, O2 and Water Vapor and Deviations from Bragg's Rule," Phys. Rev. A 29, 3419-3422 (1984).

32. L.W. Townsend, J.W. Wilson, J.W. Norbury and H.B. Bidasaria, "An Abration-Ablation Model Description of Galactic Heavy-Ion Fragmentation," NASA TP-2305 (1984).

33. J.W. Wilson,L.W. Townsend, H.B. Bidasaria , W. Schmmerling, M. Wong and J. Howard, "20Ne Depth-Dose Relations in Water," 46, 1101-1111 (1984).

34. J.W. Wilson and F.A. Cucinotta, "Human Exposure in Low Earth Orbits," NASA TP-2344 (1984).

35. An Abrasion-Ablation Model Analysis of 213 MeV/N 40Ar Fragmentation by C, VA J. Sc. 35, No. 3 (1984).

36. Pion Production Via Particle-Hole Excitations in Nucleus-Nucleus Collisions, VA J. Sc. 35, No. 3 (1984).

37. Charge-to-Mass Dispersion Methods for Abrasion-Ablation Fragmentation Models. NASA TM (1985).

38. A T-Matrix Derivation of the Abrasion-Ablation fragmentation Model. Paper presented at the 2nd International Conference on Nucleus-Nucleus Collisions, Visby, Sweden, June 1985.

39. Frictional Spectator Interaction Effects in Relativistic Argon Fragmentation by Carbon. Paper presented at the 1985 Annual Meeting of the VA Academy of Science, Williamsburg, VA, May1985.

40. A Complex T-Matrix Derivation of a Resonance Amplitude, Physics Letters, 109A, 261-264 (1985).

41. L.W. Townsend, J.W. Wilson and L.W. Norbury, "Total and Differential Cross Sections for Pion Production Via Coherent Isobar and Giant Resonance Formation in Heavy Ion Collisions", Canadian J. Phys. 63, 1242-1248 (1985).

42. J.W. Wilson and G.S. Khandelwal, "Proton Dosimeter Design for Distributed Body Organs," Nuclear Technology Journal 69, 393-394 (1985).

43. Y.J. Xu, G.S. Khandelwal and J.W. Wilson, "Proton Stopping Cross Sections for Liquid Water," Phys. Rev. A 32, 629-632 (1985).

44. J.W. Norbury, L.W. Townsend and P.A. Deutchman, " A T-Matrix Theory of Galactic Heavy-Ion Fragmentation," NASA TP-2363 (1985).

45. L.W. Townsend and J.W. Norbury, "A Simpified Optical Model Description of Heavy-Ion Fragmentation," Canadian J. Phys. 63 , 135-138 (1985).

46. F.A. Cucinotta and J.W. Wilson, "Computer Subroutines for Estimation of Human Exposure to Radiation in Low Earth Orbit," NASA TM-86324 (1985).

47. Theoretical Spectral Distributions and Total Cross Sections for Neutral Subthreshold Pion Production in Carbon-Carbon Collisions, Phys. Rev. letters, 55, 681-683 (1985).

48. A Simple Theory of LET Spectra of Heavy Ions. Paper HF1, presented at 33rd Annual Meeting of the Radiation Research Society, Los Angeles, CA, May 1985.

49. Cross Section Calculations of Subthreshold Pions in Coincidence with Giant Resonance Photons in Nucleus-Nucleus Collisions. Bull. Am. Phys. Soc. 30, 1160 (1985).

50. Y.J. Xu, G.S. Khandelwal and J.W. Wilson, "The Maximum Momentum Transfer on Proton- Hydrogen Collisions," Phys. Lett. A 115, 37-38 (1986).

51. F.A. Cucinotta, J.W. Norbory, G.S. Khandelwal and L.W. Townsend, "Doubly Differential Cross Sections for Projectile Fragmentation of 86 MeV/Nucleon C and 2.1 GeV/Nucleon O," Bull. Am.Phys. Soc. 31, 818 (1986).

52. Impulse Excitation Energies in Relativistic Heavy Ion Collisions, APS Meeting (1986).

53. J.W. Norbury and L.W. Townsend, "Electromagnetic Dissociation Effects in Galactic Heavy-Ion Fragmentation," NASA TP-2527 (1986).

54. L.W. Townsend, J.W. Wilson, F.A. Cucinotta and J.W. Norbury, "Comparison of Abrasion Model Differences in Heavy Ion Fragmentation," Phys. Rev. 34 ,1491-1494 (1986).

55. L.W. Townsend, J.W. Wilson, F.A. Cucinotta and J. W. Norbury, "Optical Model Calculations of Heavy-Ion Target Fragmentation," NASA TM-87692 (1986).

56. Theoretical Estimates of Photo-production Cross Sections for Neutral Subthreshold Pions in Carbon-Carbon Collisions, Phys.Rev. C 33, 377-378 (1986).

57. W.W. Buck, J.W. Norbury, L.W. Townsend and J.W. Wilson, " Theoretical Antideutron-Nucleus Absorptive Cross Sections," Phys. Rev. C 33, 234-248 (1986).

58. J.W. Norbury and L.W. Townsend, "Second Quantization Techniques in the Scattering of Nonidentical Composite Bodies", NASA TP-2522 (1986).

59. Theoretical Contributions to Coherent Pion Production in Subthreshold and Relativistic Heavy Ion Collisions, Nuclear Physics A 454, 733 (1986).

60. Cross Section Calculations for Subthreshold Pion Production in Peripheral Heavy Ion Collisions, NASA TP-2600 (1986).

61. Predicting Charmonium and Bottomoium Spectra with a Quark Harmonic Oscillator, Am. J. Phys. 54, 1031 (1986).

62. D-Excitations and Shell Model Information in Heavy-Ion, Charge Exchange Reactions, Phys. Rev. C 34 , 2377 (1986).

63. Towards a Quantum Mechanical Signature in Exclusive Coherent Pion Production. Phys. Rev. C (1986).

64. J.W. Wilson, L.W. Townsend and F. Badavi, " A Semiempirical Nuclear Fragmentation Model," Nuclear Instruments and Methods B18, 225-231 (1987).

65. J.W. Wilson, L.W. Townsend and F. Badavi, "Galactic HZE Propagation through the Earths Atmosphere", Radiation Research 109, 173-183 (1987).

66. Methods of Galactic Heavy Ion Transport, Radiation Research 108, 231-237 (1987).

67. Momentum Transfer in Relativistic Heavy Ion Collisions, VA J. Sc., May 20-22 (1987).

68. Eikonal Solutions to Optical Model Coupled Channel Equations for 1 GeV p-12C and 1 GeV/Nucleon 4He-12C Scattering, Bull. Am. Phys. Soc. 32, 1507 (1987).

69. Corrections to the Impulse Approximation of the First -Order Optical Potential, Bull. Am. Phys. Soc. 32 , 1566 (1987).

70. F.A. Cucinotta, J.W. Norbury, G.S. Khandelwal and L.W. Townsend, "Doubly Differential Cross Sections for Galactic Heavy-Ion Fragmentation," NASA TP-2659, 21 pages (1987).

71. L.W. Townsend, J.W. Wilson and F.A. Cucinotta, "A simple Parameterization for Quality Factor as a Function of Linear Energy Transfer," Health Physics 53, 531-532 (1987).

72. F.F. Badavi, L.W. Townsend, J.W. Wilson and J.W. Norbury, "An Algorithm for a Semi-classical Nuclear Fragmentation Model," Computer Physics Communications, 47 , 281 (1987).

73. Momentum Downshifts of Projectile Fragments in 12C Fragmentation at 2.1 A GeV in Be, C, Al, Cu, Ag and Pb Targets, Bull. Am. Phys. Soc. 33 , 2193 (1988).

74. A General Formalism for Phase Space Calculations, NASA TP-2843 (1988).

75. Accuracy of Analytic Energy Level Formulas Applied to Hadronic Spectroscopy of Heavy Means, NASA TM-4042 (1988).

76. J.W. Wilson, L.W. Townsend, B.D. Ganapol and S.L. Lamkin, "Methods for High Energy Hadronic Beam Transport," Trans. American Nuclear Soc. 56, 271-272 (1988).

77. F. Khan, G.S. Khandelwal, J.W. Wilson, L.W. Townsend and J.W. Norbury, "Excitation Decay Contribution of Projectile Fragments to (12c, 11B+P) Cross Section at 2.1 A GeV with 12C Targets," Proceeding of Eighth High Energy heavy ion Study, published by Lawrence Berkely Laboratory, 440-449, Jan. (1988).

78. F. Khan, G.S. Khandelwal and J.W. Wilson, " 1s2 1S-1s np1P Transitions of the Helium ISO Electronic Sequence Members up to z=30," Astrophys. J. 329, 493-497 (1988).

79. F. Khan, G.S. Khandelwal and J.W. Wilson, "Static Multipole Polarizabilities and Second- OrderStark Shift in Francium," J. Phys. B, At. Mol. Opt. Phys. 21, 731-737 (1988).

80. J.W. Wilson, G.S. Khandelwal and N.T. Fogarty, "X-Ray Production in Low Energy Proton Stopping," NASA TM 100619,10 pages (1988).

81. F.A. Cucinotta, G.S. Khandelwal, K.M. Maung, L.W. Townsend and J.W. Wilson, "Eikonal Solutions to Optical Model Coupled Channel Equations," NASA TP-2830, 27 pages (1988).

82. F.A. Cucinotta, J.W. Norbury and L.W. Townsend, "Multiple Nucleon Knockout by Coulomb Dissociation in Relativistic Heavy-Ion Collisions," NASA TM-4070 (1988).

83. D. Olsgaard, F. Khan and G.S. Khandelwal, "Asymptotic Screened Hydrogenic Radial Integrals," J. of the Optical Soc. of Am. 5, 2437 (1988).

84. F. Khan, G.S. Khandelwal and J.W. Wilson, "Differential Oscillator Strengths and Dipole Polarizabiliities for Transitions of the Helium Sequence," Phys. Rev. A 38, 6159 (1988).

85. J.W. Norbury, L.W. Townsend and F.F. Badavi, "Computer Program for Parameterization of Nucleus-Nucleus Electromagnetic Dissociation Cross Sections," NASA TM-4038 (1988).

86. J.W. Wilson, L.W. Townsend, S. Y. Chun, W.W. Buck, F. Khan and F.A. Cucinotta, "BRYNTRN: A Baryon Transport Computer Code; Computation Procedures and Data Base," NASA TM-4037 (1988).

87. J.W. Norbury, F.A. Cucinotta, L.W. Townsend and F.F. Badavi, "Parameterized Cross Sections for coulomb Dissociation on Heavy Ion Collisions," Nuclear Instruments and Methods B 31, 535-537 (1988).

88. J.W. Wilson, L.W. Townsend, B. Ganapol, S.Y. Chun and W.W. Buck, "Charge Particle Transport in One Dimension, Nuclear Science and Engineering," 99, 285-287 (1988).

89. J.W. Wilson, L.W. Townsend and F. Khan, "Evaluation of Highly Ionizing Components in High- Energy Nucleon Radiation Fields," Health Physics 57, 717-724 (1989).

90. Corrections to Pole Diagram in 4He Fragmentation at 1 GeV/A, APS Bull. 34, 1138 (1989).

91. F.A. Cucinotta, G.S. Khandelwal, L.W. Townsend and J.W. Wilson, "Correlations in a-a Scattering and Semi-Classical optical Models," Phys. Lett. B 223, 127 (1989).

92. G.S. Khandelwal, F. Khan and J.W. Wilson, "An Asymptotic Expression for Dipole Oscillator Strength for Transitions of He Sequence," Astrophys. J. 336, 504 (1989).

93. G.S. Khandelwal, W.M. Pritchard, G. Grubb and F. Khan, "Screened Hydrogenic Radial Integrals," Phys. Rev. A 39, 3960 (1989).

94. Pseudo-Scalar pN Coupling and Relativistic Proton-Nucleus Scattering, Phys. Rev. C 40, R10- R12 (1989).

95. Y.J. Xu, G.S. Khandelwal and J.W. Wilson, "Charge Exchange Transition Probability for Collisions Between Unlike Ions and Atoms Within the Adiabatic Approximation," NASA TM-101559, 42 pages (1989).

96. J.W. Wilson, S.L. Lamkin, H. Farahat, B.D. Ganapol and L.W. Townsend, "A Hiarchy of Transport Approximations for High Energy Heavy (HZE) Ions," NASA TM-4118 (1989).

97. J.W. Wilson, L.W. Townsend, J.E. Nealy, S.Y. Chun, B.S. Hong, W.W. Buck, S.L. Lamkin, B.D. Ganapol. F. Khan and F.A. Cucinotta, "BRYNTRN: A Baryon Transport Model," NASA TP- 2887 (1989).

98. Collision Impact Parameter Estimates for Fragmentation of 1.2A GeV 139La Nuclei on Carbon. Division of Nuclear Phys. Fall Meeting, APS, Oct. 12-14, 1989.

99. J.W. Wilson, G.S. Khandelwal, J.L. Shinn, J.E. Nealy, L.W.Townsend and F.A. Cucunotta, "Simplified Model for Solar Cosmic Ray Exposure in Manned Earth Orbital Flights, NASA TM- 4182, 12 pages (1990).

100. F. Khan, G.S. Khandelwal and J.W. Wilson, "Moments of the Oscillator Strength Distribution of the Helium Isoelectronic Sequence," J. Phys. B: At.Mol.opt. Phys. 23, 2717-2726 (1990).

101. F. A. Cucinotta, L. W. Townsend, J. W. Wilson, and G. S. Khandelwal, " Inclusive Inelastic Scattering of Heavy Ions and Nuclear Correlations, NASA Technical Paper # 3026, 17pages, November (1990).

102 F. Khan,G.S. Khandelwal, L.W. Townsend, J.W. Wilson, and J.W. Norbury, " Estimates of Fragment Momentum Distributions for Carbon Ions at 250 A MeV," Bull. Am. Phys. Soc. April 1990.

103. Momentum Transfer in Heavy-Ion Charge Exchange Reactions, Spring Meeting, Bull. Am. Phys. Soc. 35 , 999 (1990).

104. L.W. Townsend, F. Khan, G.S.Khandelwal, and J.W. Wilson, " Momentum Downshifts in Heavy-Ion Charge Exchange Reactions," Bull. Am. Phys. Soc. April, 1990.

105. F. Khan, G.S. Khandelwal, L.W. Townsend, and J.W. Wilson, " Resonant Excitation of Vibrational Levels as the Origin of Positron Peaks," Proceedings of the 12th International Conference on Particles and Peaks, June, 1990.

106. J.W. Wilson, et al., "A Closed Form Solution to HZE Propagation", Radiation Research, Vol. 122, No.2, May 1990, pp.223-228.

107. Optical Model Calculations of 28Si Fragmentation at 14.6 A GeV. Bull. Am. Phys. Soc. 36, 8 (1991).

108. An Energy Dependent Semiempirical Nuclear Fragmentation Model. Bull. Am. Phys. Soc. 36, 8 (1991).

109. R. Dubey, G.S. Khandelwal, F. Cucinotta and L.W. Townsend, " Parameterization of Off-Shell Alpha-Alpha Transition Amplitude," Va. Academy of Science, page 23, may, 1991.

110. The Evaluation of Kerma Values for Hydrogen, Carbon, Nitrogen and Oxygen, Va. J. Science (1991).

111. R. Dubey, G.S. Khandelwal and W.M. Pritchard, "Asymptotic Expansions of the Hydrogenic Radial Dipole Integrals", J. Physics B: At.Mol.opt Phys. 24, 57-63 (1991).

112. F. Khan, G.S. Khandelwal, L.W. Townsend, J.W. Wilson and J.W. Norbury, "An Optical Model Description of Momentum Transfer in Heavy Ion Collisions," Physical Rev. C, 43, 1372-77 (1991).

113. L.W. Townsend, J.W. Wilson, F. Khan and G.S. Khandelwal, "Momentum Transfer in Relativistic Heavy Ion Charge-Exchange Reactions," Physical Rev. C, 44, 540 - 542 (1991).

114. J. W. Wilson, L. W. Townsend, W. Schimmerling, G. S. Khandelwal, Khan, J. E. Nealy, F. A. Cucinotta, L. C. Simonsen, J. L. Shin and J. W. Norbury," Transport Methods and Interactions for Space Radiations," NASA RP - 1257 (1991) 606 pages.

115. B.D. Ganapol, L.W. Townsend, S.L. Lamkin and J.W. Wilson, "Benchmark Solutions for the Galactic Heavy-Ion Transport Equations With Energy and Spatial Coupling," NASA TP-3112 (1991).

116. J.W. Wilson , S.Y. Chun, F.F. Badavi, L.W. Townsend and S.L. Lamkin, "HZETRN: A heavy Ion/Nucleon Transport Code for Space Radiations," NASA TP-3146 (1991).

117. An Optical Model Description of Transverse Momentum Transfer and "Sideways Flow" in Relativistic Heavy Ion Collisions. Bull. Am. Phys. Soc. 36 , 1402 (1991).

118. Optical Model Description of Collective Flow and Flow Angles in Intermediate and High Energy Heavy-Ion Collisions. Bull. Am. Phys. Soc. 36, 2152 (1991).

119. Calculation of Hadronic Dissociation of 28Si Projectiles at 14.6 A Gev by Nucleon Emission. Physical Review C 43, 2045 (1991).

120. NUCFRAG: A semi-empirical HZE Particle Fragmentation Model. 40th Annual Meeting of the Radiation Research Society, Salt Lake City, UT, March 1992.

121. F.A. Cucinotta, S.M. Beck, L.W. Townsend, J.W. Wilson, R.K. Tripathi and R.R. Dubey, "Final State Interaction Effects on the Quasi-Elastic Peak for Proton-Nucleus Scattering, "Bull. Am. Phys. Soc. (1992).

122. R. Dubey, G. Khandelwal, F. A. Cucinotta, and L. W. Townsend, " Final State Interaction Effects on the Quasi-Elastic Peak for Proton-Nucleus Scattering," Va. Acad. Of Science, Page 17, May, 1992.

123. Argon Fragmentation at 1.65 A GeV I. Optical Model Cross Sections. Bull. Am. Phys. Soc. 37, 1003 (1992).

124. Argon Fragmentation at 1.65 A GeV II. Semiempirical Model Cross Sections. Bull. Am. Phys. Soc. 37, 1002 (1992).

125. Argon Fragmentation at 1.65 A GeV III. Momentum Distributions. Bull. Am. Phys. Soc. 37, 901 (1992).

126. Multiple-Scattering Model for Quasi-Elastic Alpha-Nucleus Collisions, Bull. Am. Phys. Soc. 37, 901 (1992).

127. Computational Efficient Space Radiation Transport Codes, Proceedings of the American Nuclear Society, Tropical Meeting on New Horizons in Radiation Protection and Shielding, Pasco, WA, 1992.

128. Is There Universality in Flow Phenomena in Heavy-Ion Collisions? Advances in Nuclear Dynamics: Proceedings of the 8th Winter Workshop in Nuclear Dynamics, Dec. 1992.

129. In- Medium Effects in the Disappearance of Collective Flow, Division of Nuclear Physics Meeting, Santa Fe, NM, Oct., 1992. Published in Bull. APS.

130. Mean-filed Momentum Dependence and Transverse Momentum Transfer in the Optical Model. Division of Nuclear Physics Meeting, Santa Fe., NM, Oct., 1992, published in the Bull. APS.

131. S. Lamkin, G. S. Khandelwal and J. W. Wilson," Numerical Methods for High Energy Nuclear Transport," Proceedings Am. Nucl. Soc. (1992) pages 165-170.

132. BOOK LENGTH PAPER; J.W. Wilson, L.W. Townsend, W. Schimmerling, G.S. Khandelwal, F. Khan, J.E. Nealy, F.A. Cucinotta, L.C. Simmsen, J.L. Shin, and J.W. Norbury, "Transport Methods and Interactions for Space Radiations," (pp. 1187-1787) in Biological Effects and Physics of Solar and Galatic Cosmic Radiations, Part B; ed. by C.E. Swenburg, G. Homuk, and E.G. Stassinopoulos; Plenum Pub. (1993).

30

133. J.W. Wilson, S.Y. Chun, F.F. Badavi and S. John, "Coulomb Effects in Low-Energy Nuclear Fragmentation," NASA TP-3352 (1993).

134. F.A. Cucinotta and R.R. Dubey, "Final State Interactions and Inclusive Nuclear Collisions," NASA TP-3353 (1993).

135. F.A. Cucinotta, L.W. Townsend and R.R. Dubey, "Energy-Loss Cross Sections for Inclusive Nuclear Collisions," NASA TP-4522 (1993).

136. R. Dubey, G. Khandelwal, F. Cucinotta, and K. Maung, "Nucleus -Nucleus scattering using the First Order Optical Potential," Bull. Am. Phys. Soc. 38, 1834 (1993).

137. L.W.Townsend, J.W. Wilson, R.K. Tripathi, J.W. Norbury, F.F. Badavi and F. Khan, " HZEFRG1: An Energy-Dependent Semiempirical Nuclear Fragment Model," NASA TP-3310 (1993).

138. Fragment Mass-Dependence of Transverse Momentum Transfer: Men Field vs. NN Collision Dynamics, Joint April Meeting of the APS and AAPT, Washington, D.C., April 1993.

139. Optical Model Calculations of 14.6 A GeV Silicone Fragmentation Cross Sections. NASA TM-4461 (1993).

140. Widths of Transverse Momentum Distributions in Intermediate-Energy Heavy Ion Collisions. Physical Review C, 48, 926-928 (1993).

141. Momentum Loss in Proton-Nucleus and Nucleus-Nucleus Collisions. NASA TP-3405 (1993).

142 F.A. Cucinotta and R.R. Dubey, "Alpha-Cluster Description of Excitation Energies in 12C(12C, 3a)X at 2.1 A GeV," Phys. Rev. C50, 1090-1096 (1994).

143. J.W. Wilson, J.L. Shinn, L.W. Townsend, R.K. Tripathi, F.F. Badavi and S.Y. Chun, "NUCFRG2: A Semiempirical Nuclear Fragmentation Model," Nuclear Instruments and Methods in Physics Research B 94, 95-102 (1994).

144. S.L. Lamkin, G.S. Khandelwal, J.L. Shinn, and J.W. Wilson, "Space Proton Transport in One Dimension," Nuclear Science and Engineering, 116, 291-299, (1994).

145. R. Dubey, G, Khandelwal, F. Cucinotta, and L. Townsend, " Model for Multiple Knockout during Quasi- Elastic Charge Exchange Reactions," Bull. Am. Phys. Soc. 39, 1139, April 1994.

146. S. Y. Chun, G. S. Khandelwal, J. W. Wilson, and F. F. Badawi, " Development of a Fully Energy- Dependent HZE Greens Function," Proceedings, 8th International Conference on Radiation Shielding, Am Nuclear Soc. 625-632, April 1994.

147. R. Dubey, G. Khandelwal, F. Cucinotta, and K. Maung, " Comparison of Exact Solution with Eikonal Approximation for Elastic Heavy Ion Scattering," NASA Technical Paper 3498, 15 pages, February 1995.

148. R. Dubey, G. Khandelwal, F. Cucinotta, and J. W. Wilson, " a-Clustering Effects in the Fragmentation of Heavy-Ions," Bull. Am. Phys. Soc. 40, 1618, October 1995.

149. Light Ion Components of the Galactic Cosmic Rays: Nuclear Interaction, Adv. Space Res. 17 , 77 (1995).

150. F.A. Cucinotta, K. Katz, J.W. Wilson and R.R. Dubey, "Heavy Ion Track Strucure Calculation for Radial Dose in Arbitrary Materials," NASA TP-3497 (1995).

151. F.A. Cucinotta, L.W. Townsend, J.W. Wilson, J.L. Shin, G.D. Badhwar and R.R. Dubey, "Light Ion Components of the Galactic Cosmic Rays: Nuclear Interactions and Transport Theory," Adv. Space Res. 17, 77 (1995).

152. a-Production Cross Section in Heavy-Ion Fragmentation Under Abrasion-Ablation Models. Paper presented at the joint meeting of CAP (Canada) and SMF (Mexico), June 1995.

153. F.A. Cucinotta, J.W. Wilson, K.M. Maung, T. Christian, R.K. Tripathi and R.R. Dubey, "Nuclear Interactions Models in the Development of Cross Section Libraries for Cosmic Ray Studies," Radiation Protection and Shielding, Tropical Meeting (1996).

154. F.A. Cucinotta, L.W. Townsend, J.W. Wilson, J.L. Shinn, G.D. Badhwar and R.R. Dubey, "Light Ion Components of the Galactic Cosmic Rays: Nuclear Interactions and Transport Theory," Adv. Space Res. 17 , 77-86 (1996).

155. R. Dubey, G. Khandelwal, F. Cucinotta, and J. Wilson, " Microscopic Optical Model Calculations of Heavy Ion Absorption Cross-Sections," J. Phys. G: Nucl. Part. Phys. 22, 387-396 (1996).

156. S. Y. Chun, G. S. Khandelwal, and J. W. Wilson, " A Greens Function Method for High Charge and Energy Ion Transport," Nuclear Science and Engineering: 122, 267-275 (1996).

157. J.L. Shinn, F.A. Cucinotta, L.C. Simonsen, J.W. Wilson, F.F. Badavi, G.D. Badhwar, J.Miller, C. Zeitlin, L. Heilbronn, R.K. Tripathi, M.S. Clowdsley, J.H. Heinbockel, M.A. Xapsos., "Validation of a Comprehensive Space Radiation Transport Code", IEEE Nuclear and Space Radiation Effects Conference, Newport Beach, California, July 20-24, 1998. (To appear in the IEEE Transcations on Nuclear Science Journal, December 1998.)

158. Judy L. Shinn, John W. Wilson, M.A. Lone, P.Y. Wong and Robert C. Costen, "Preliminary Estimates of Nucleon Fluxes in a Water Target Exposed to Solar-Flare Protons: BRYNTRN Versus Monte Carlo Code.", NASA Technical Memorandum 4565, June 1994.

APPENDIX B

The research grant NCC 1-42 has produced the
following Ph.D. students and their associated thesis work.

1. A Theoretical Model of Calculation of Molecular Stopping Power, Y.J. Xu, Ph.D Dissertation (1984).

2. Radiation Damage to GAAs Solar Cells Including Isotropic Effects, L.V. Stock, M.S. Thesis (1984).

3. Theory of Alpha-Nucleus Collisions at High Energies, F.A. Cucinotta, Ph.D Dissertation (1988).

4. Nuclear Fragmentation Energy and Momentum Transfer Distributions in Relativistic Heavy-Ion Collisions, F. Khan, Ph.D Dissertation (1989).

5. The Study of Oxygen Transport through Polycrystalline Single Crystal and alloyed Silver, D. Wu, M.S. Thesis (1990).

6. High Energy Coupled Nucleon Transport in One Dimension, S. L. Lamkin, Ph.D Dissertation (1994).

7. Dosimetry of High-Energy Heavy-Ion Beams using Energy-Dependent Greens Functions, S. Y. Chun, Ph.D. Dissertation (1994).

8. Heavy-Ion Interaction Models for Radiation Transport, Rajendra R. Dubey, Ph.D Dissertation (1995).

9. Numerical Solution of the Low Energy Neutron Boltzmann Equation, M.S. Clowdsley, Ph.D Dissertation (1998).
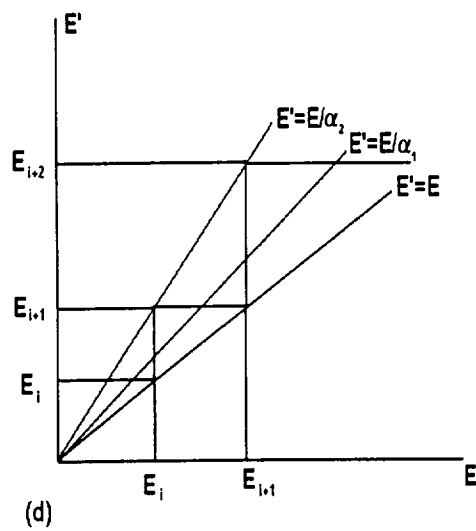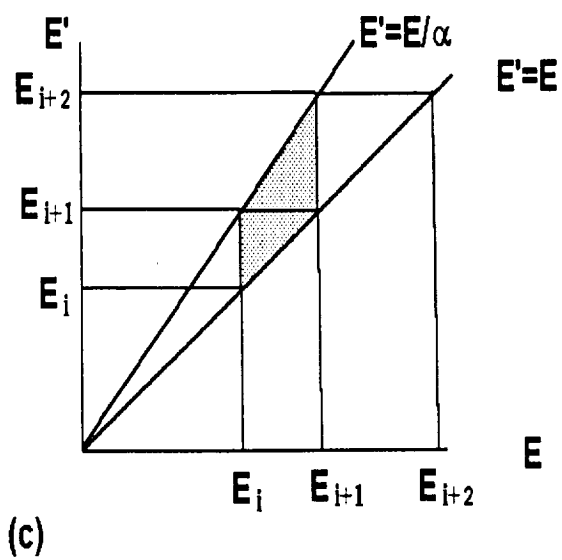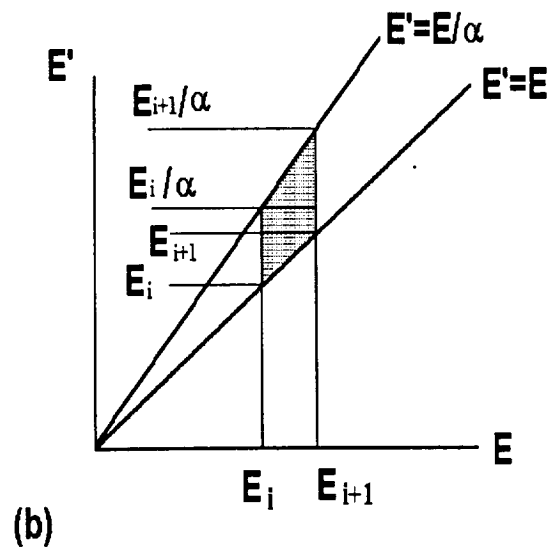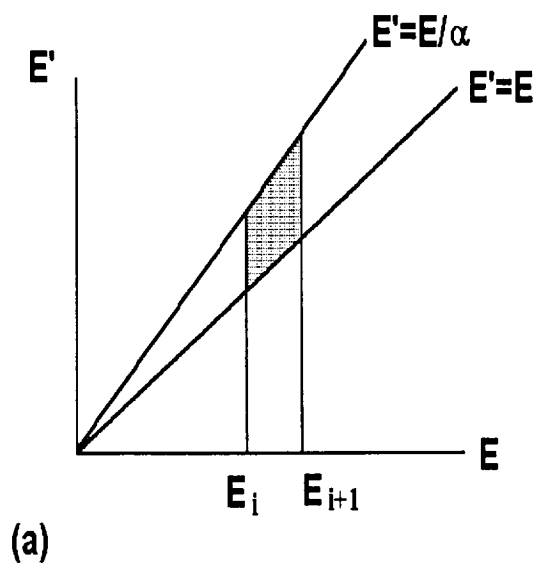
Figure 1. Energy partitioning

35

$$[E_0, E_1, ..., E_{n-1}, E_n, E_{n+1}]$$

$$[E_0, E_1, ..., E_{n-1}, E_n, E_{n+1}]$$

$$[\quad - - - , E_n, E_{n+1}]$$

$$- - -$$

$$[E_0, E_1, ..., E_{n-1}, E_n, E_{n+1}]$$
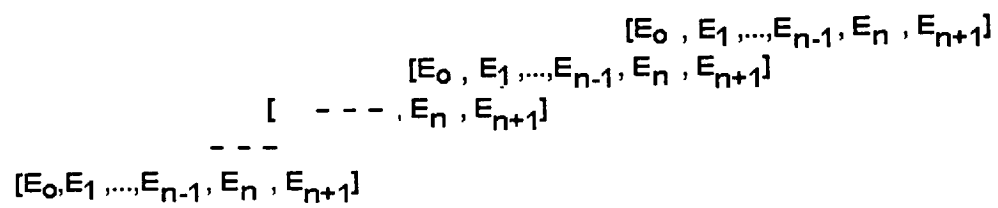
Figure 2. Overlapping last position of multiple energy groups
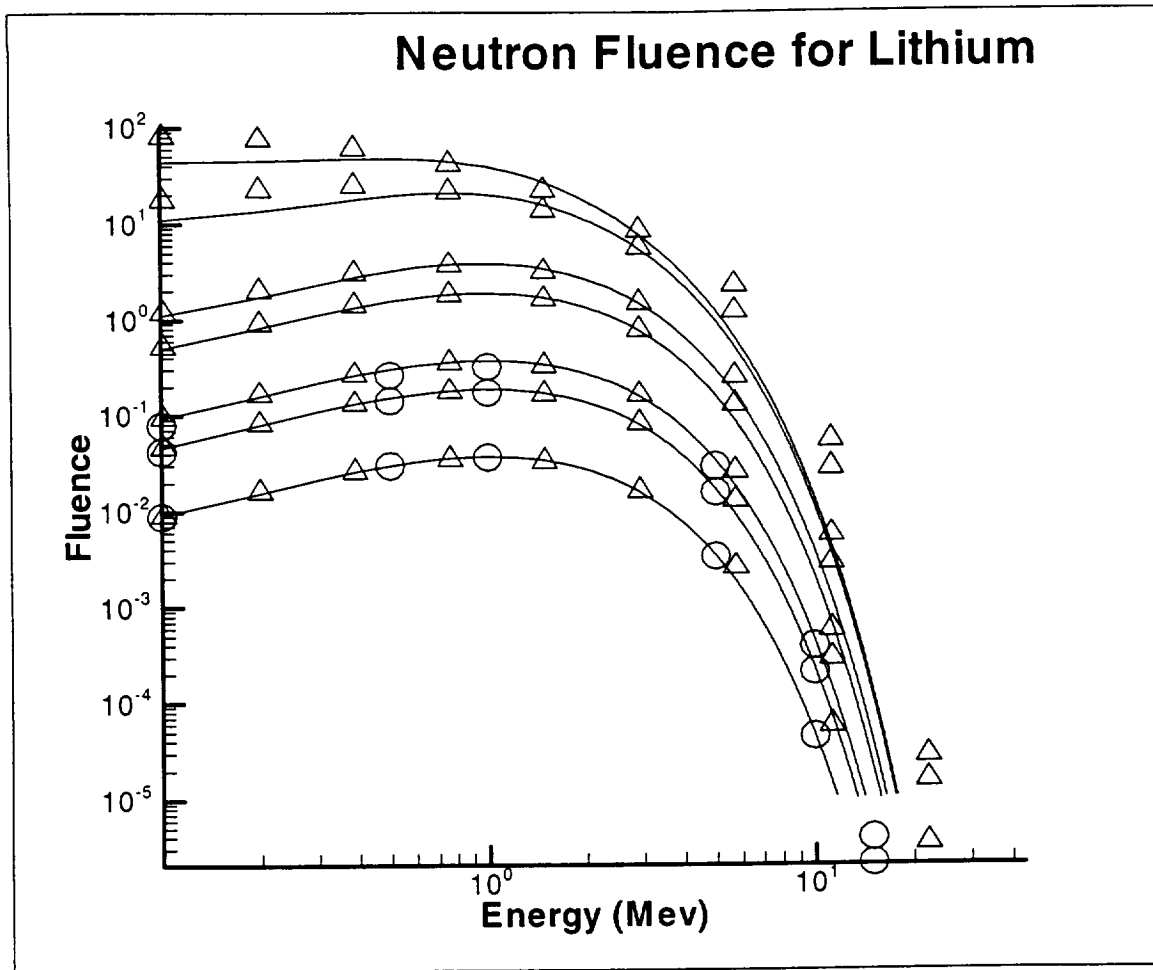
Figure 3. Comparison of numerical solution with multigroup solution (n=2) for lithium.
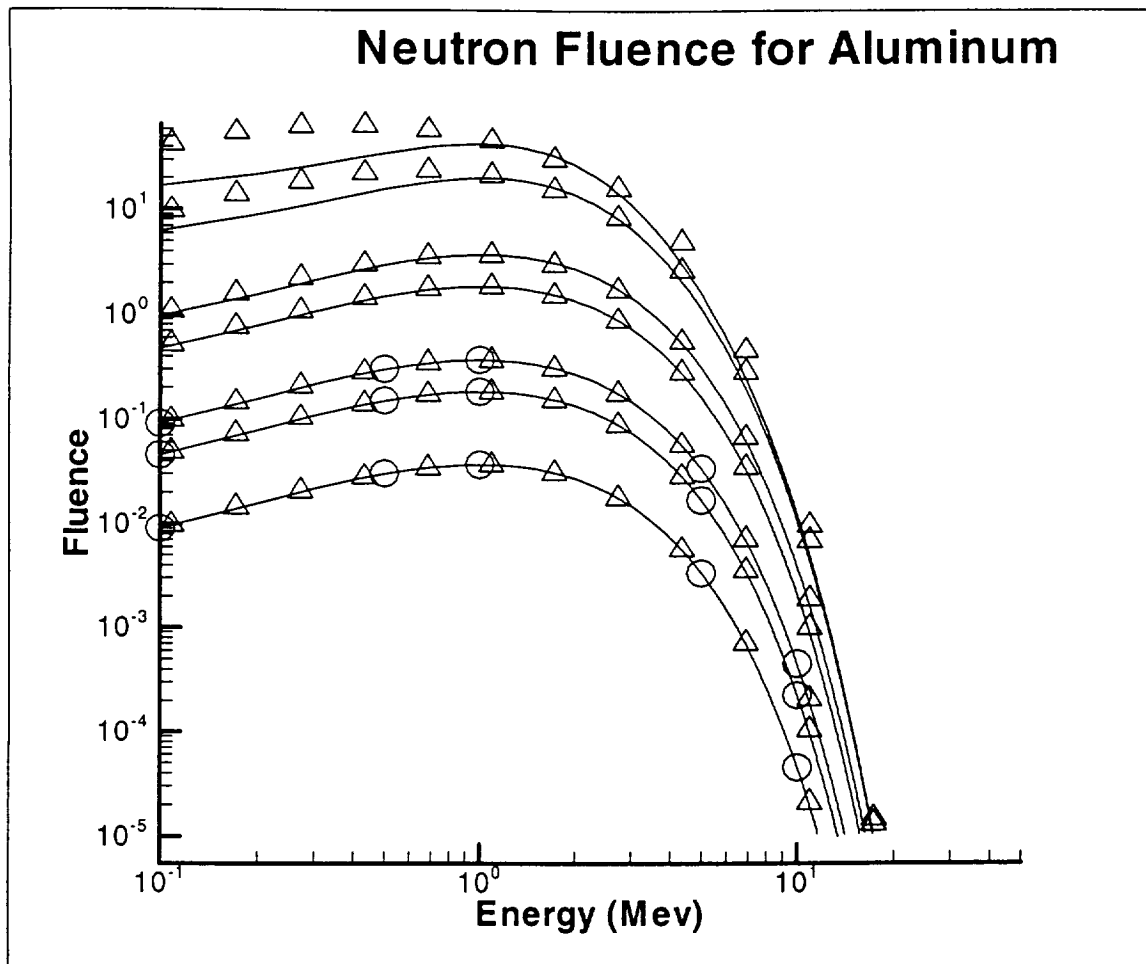
Figure 4. Comparison of numerical solution with multigroup solution (n=2) for aluminum.
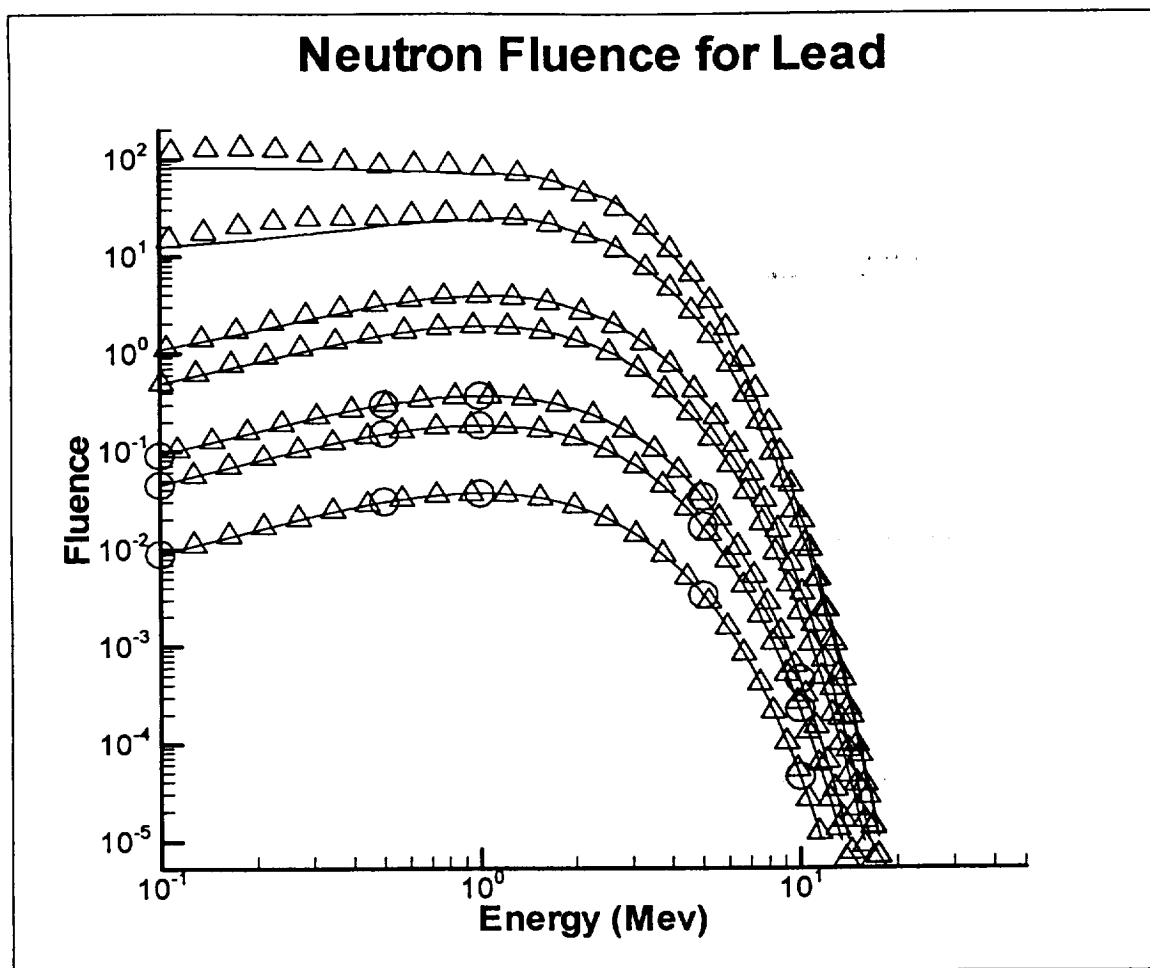
Figure 5. Comparison of numerical solution with multigroup solution (n=2) for lead.
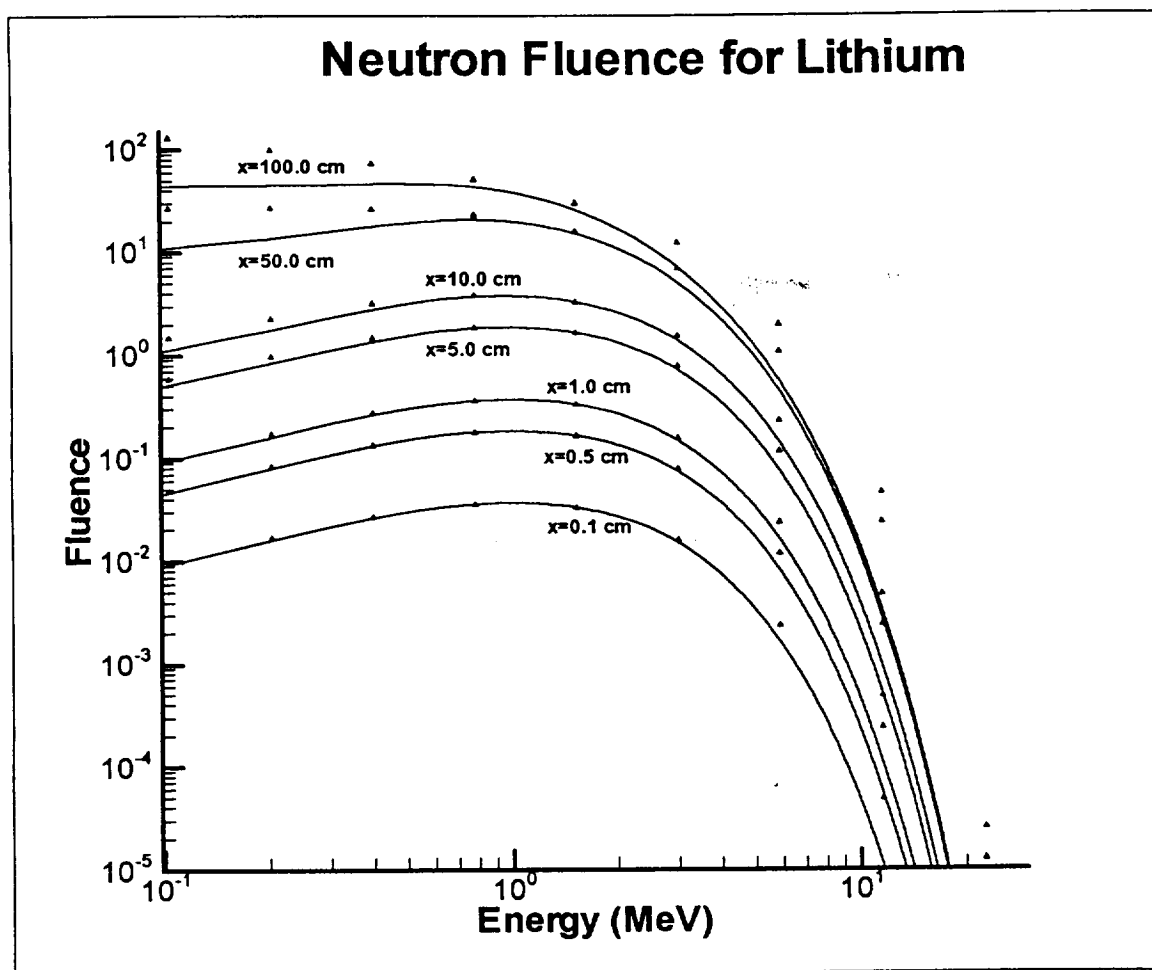
Figure 6. Comparison of numerical solution with multigroup solution (n=10) for lithium.
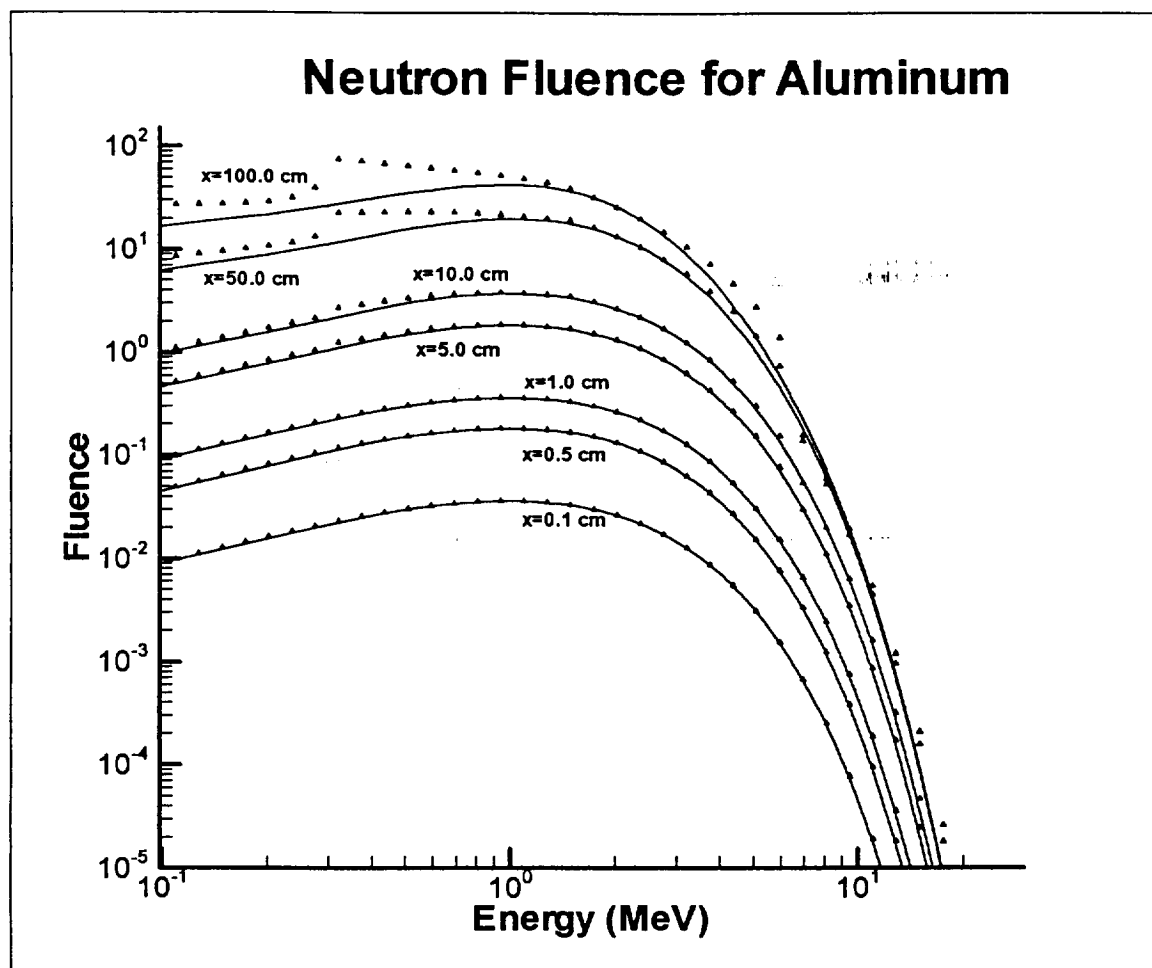
Figure 7. Comparison of numerical solution with multigroup solution (n=10) for aluminium.
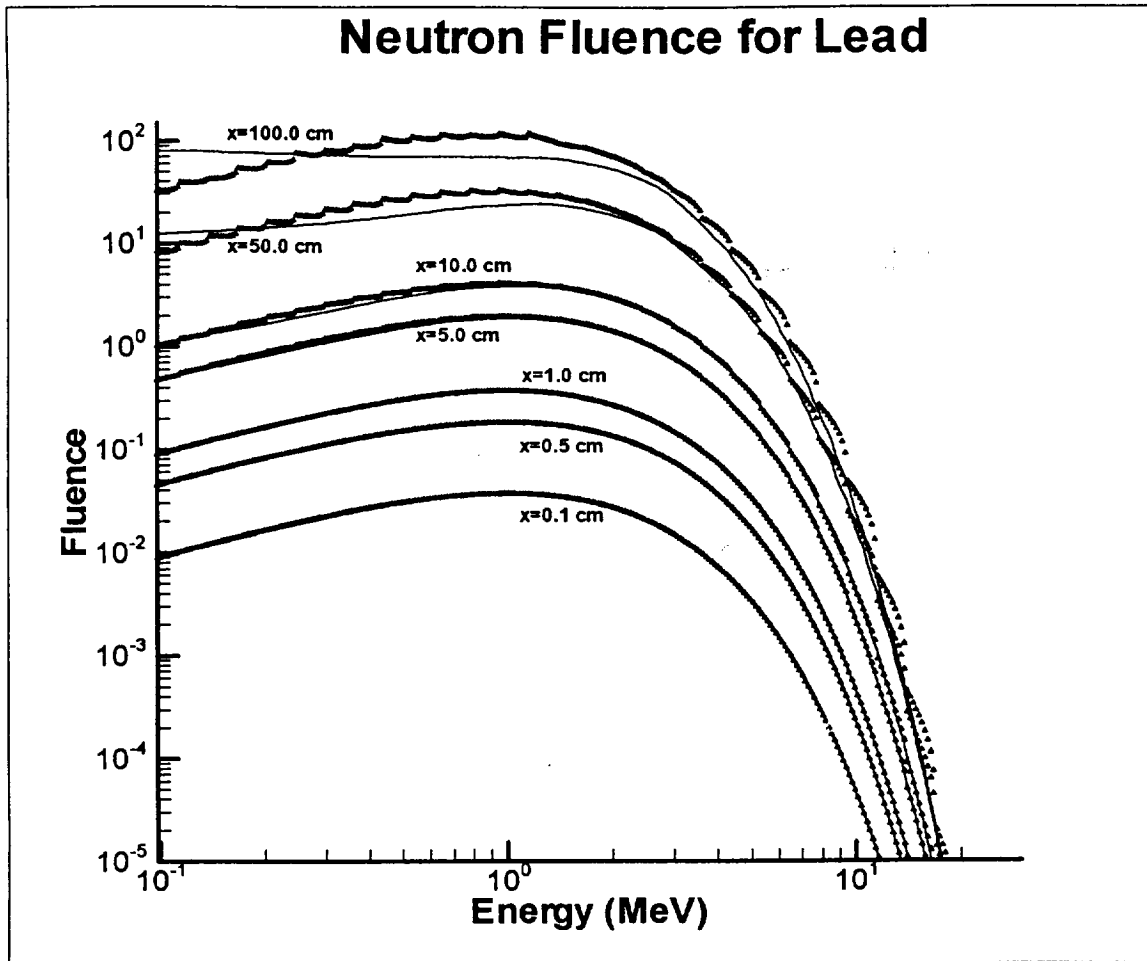
Figure 8. Comparison of numerical solution with multigroup solution (n=10) for lead.
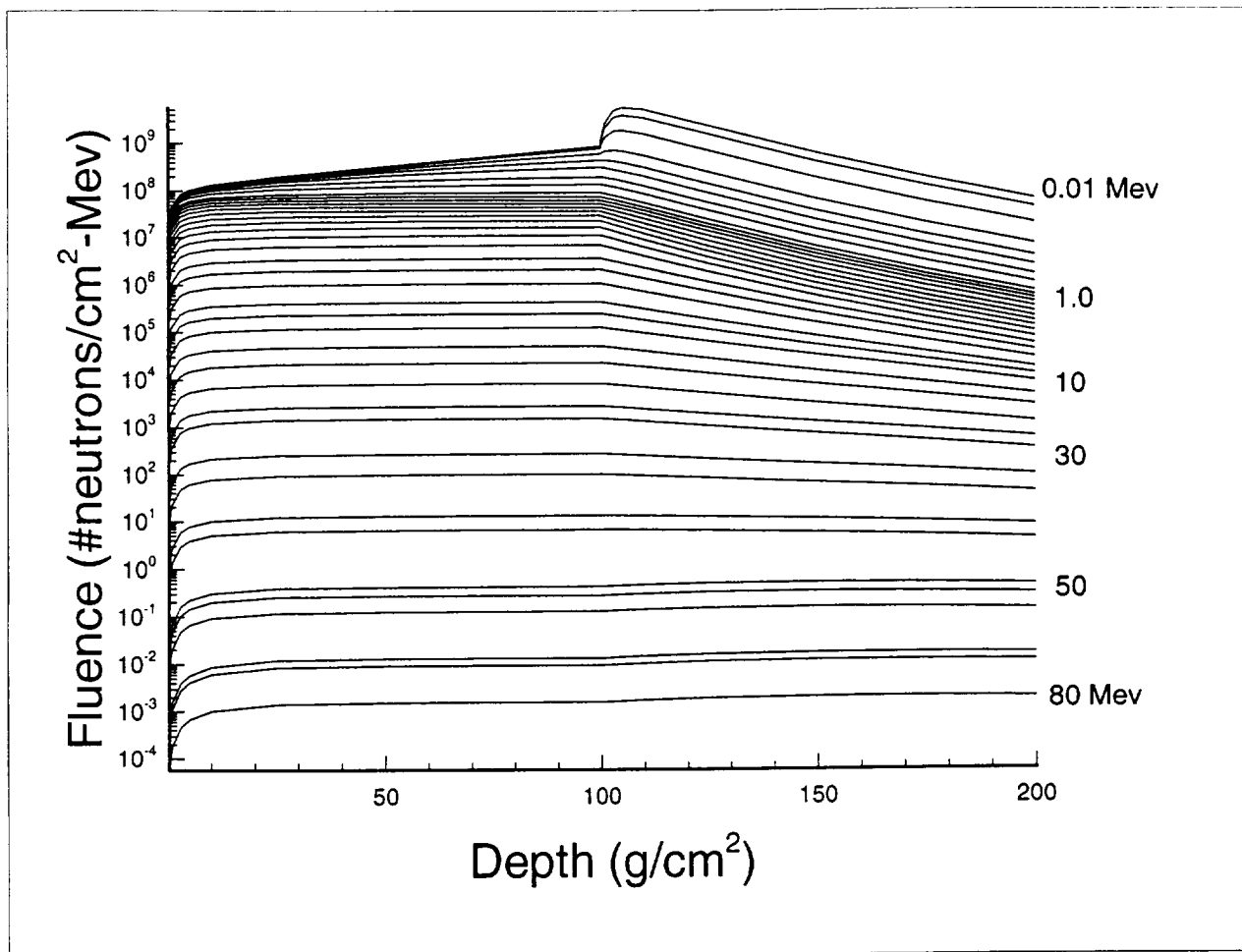
Figure 9. Multi-group low energy evaporation neutron fluence vs depth in shield-target configuration for various energies.
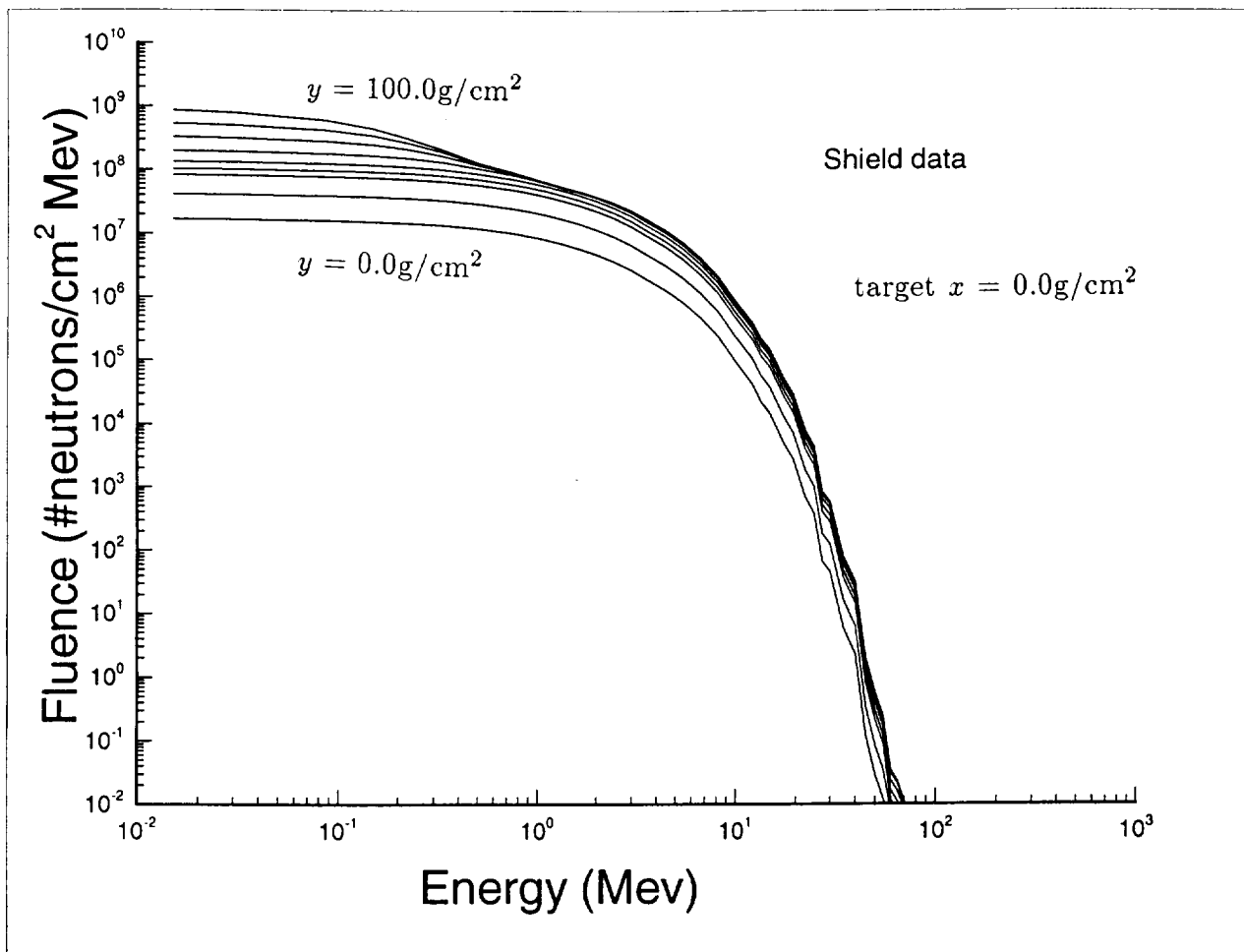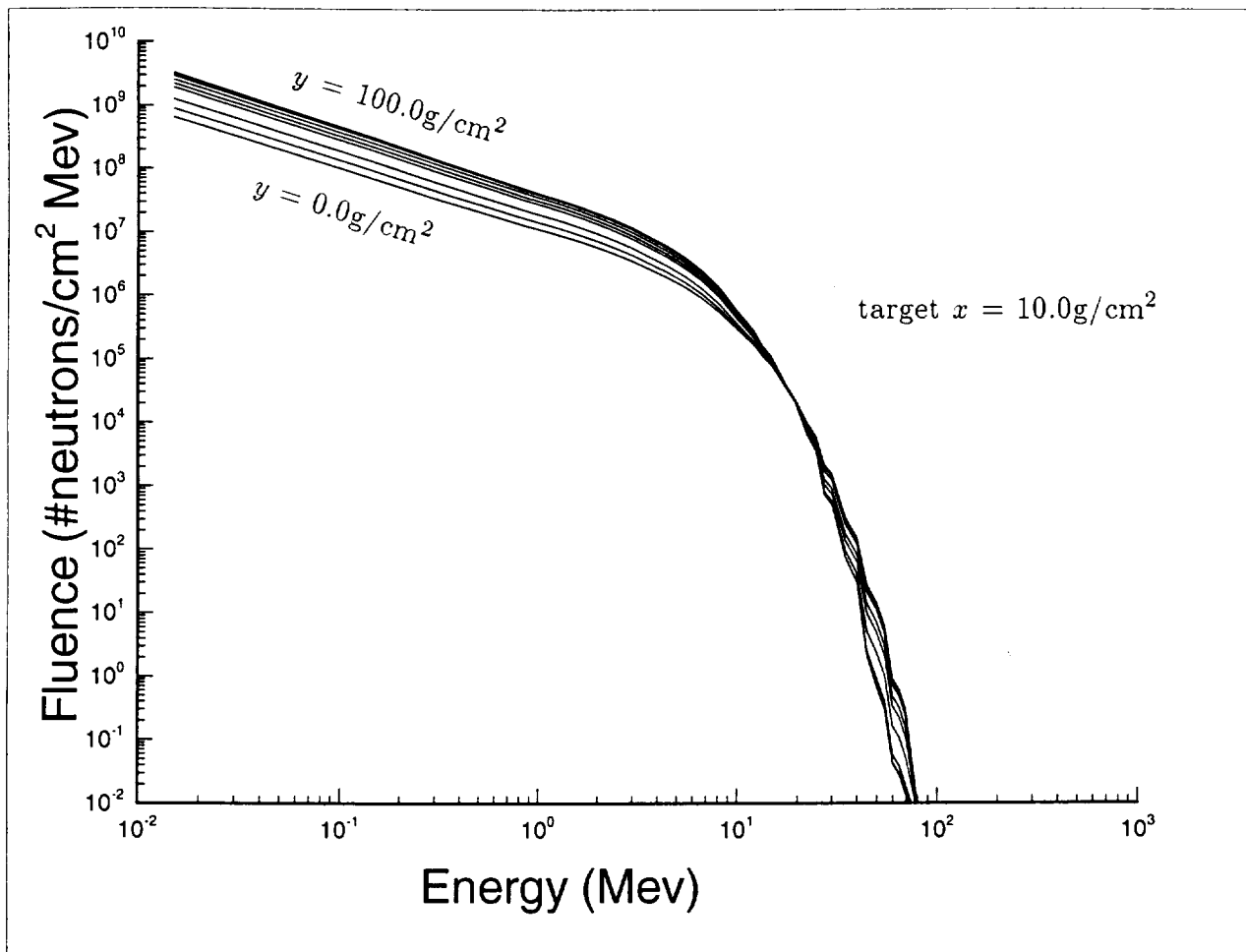
Figure 10. Multi-group low energy evaporation neutron fluence
vs energy for target 0.0 g/cm^2 and various shield thicknesses.
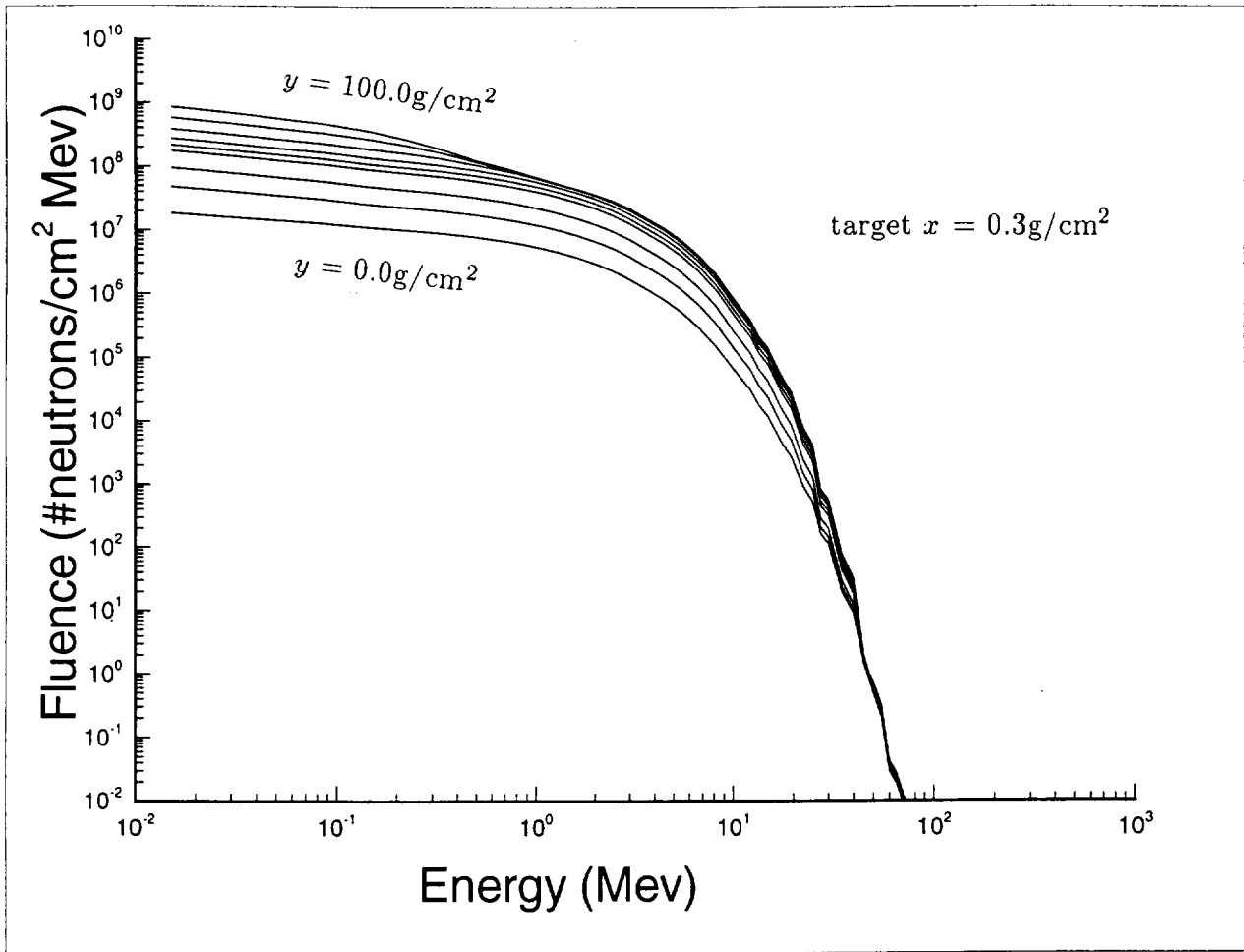
Figure 11. Multi-group low energy evaporation neutron fluence vs energy for target 0.3 g/cm^2 and various shield thicknesses.
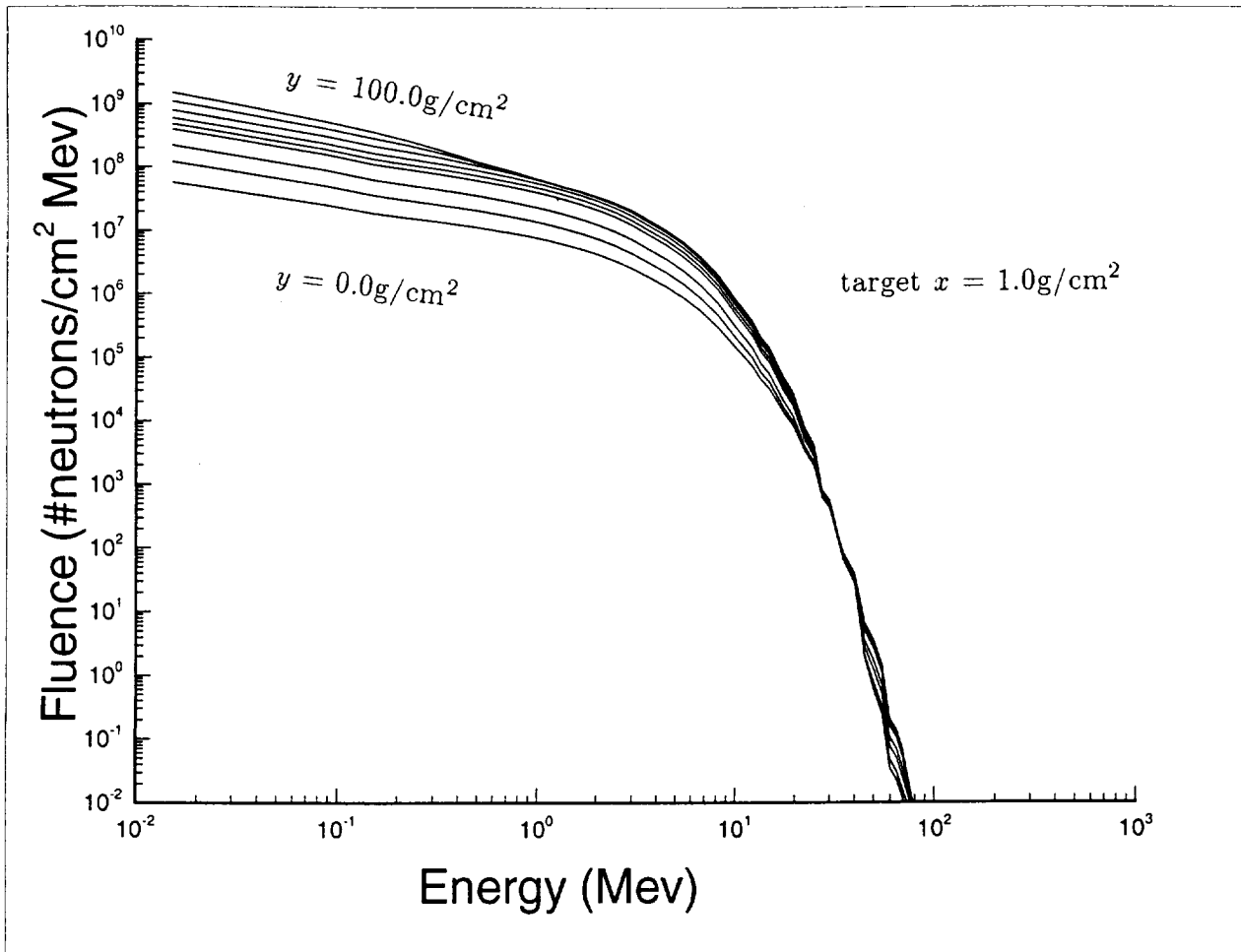
Figure 12. Multi-group low energy evaporation neutron fluence
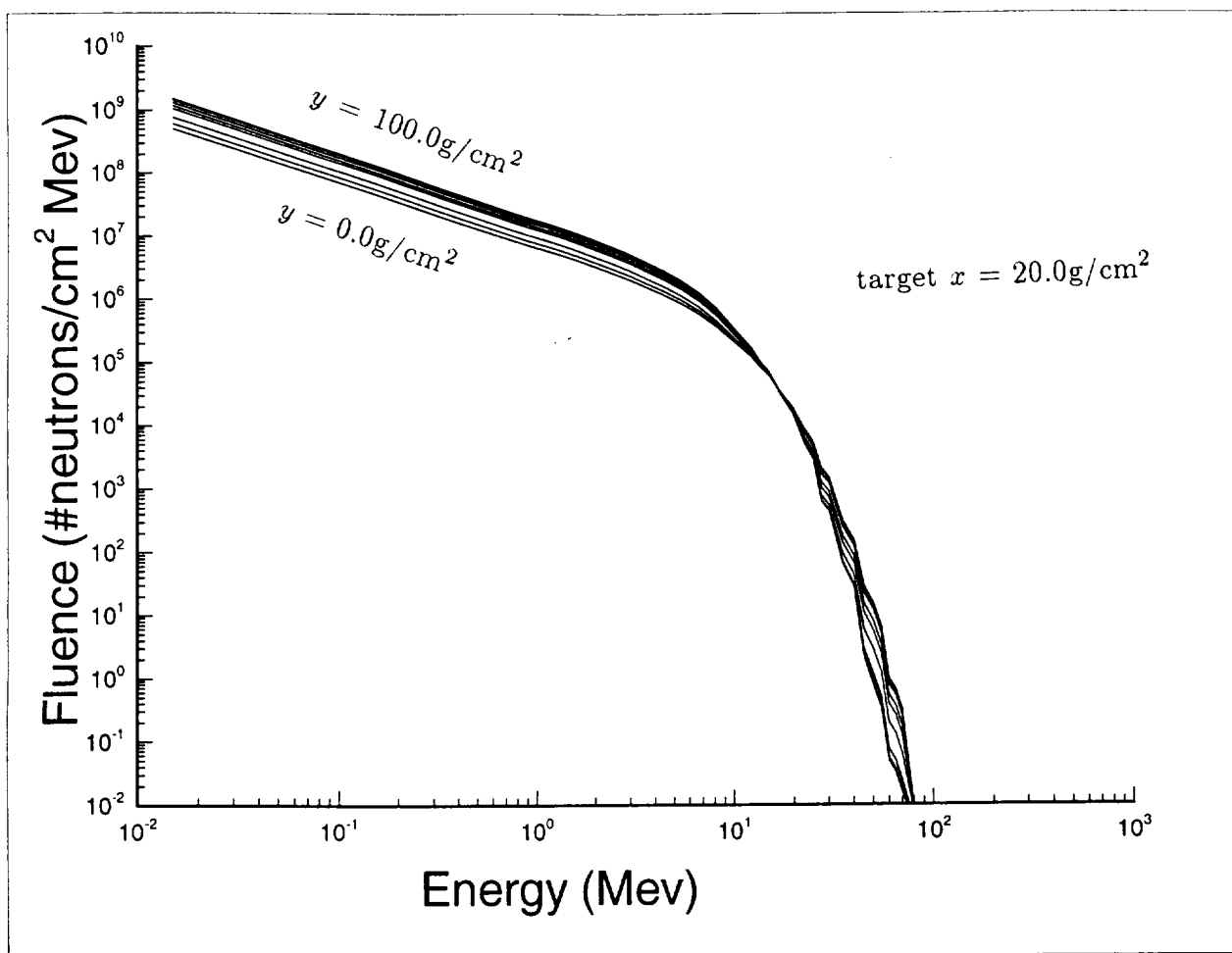vs energy for target 1.0 g/cm^2 and various shield thicknesses.
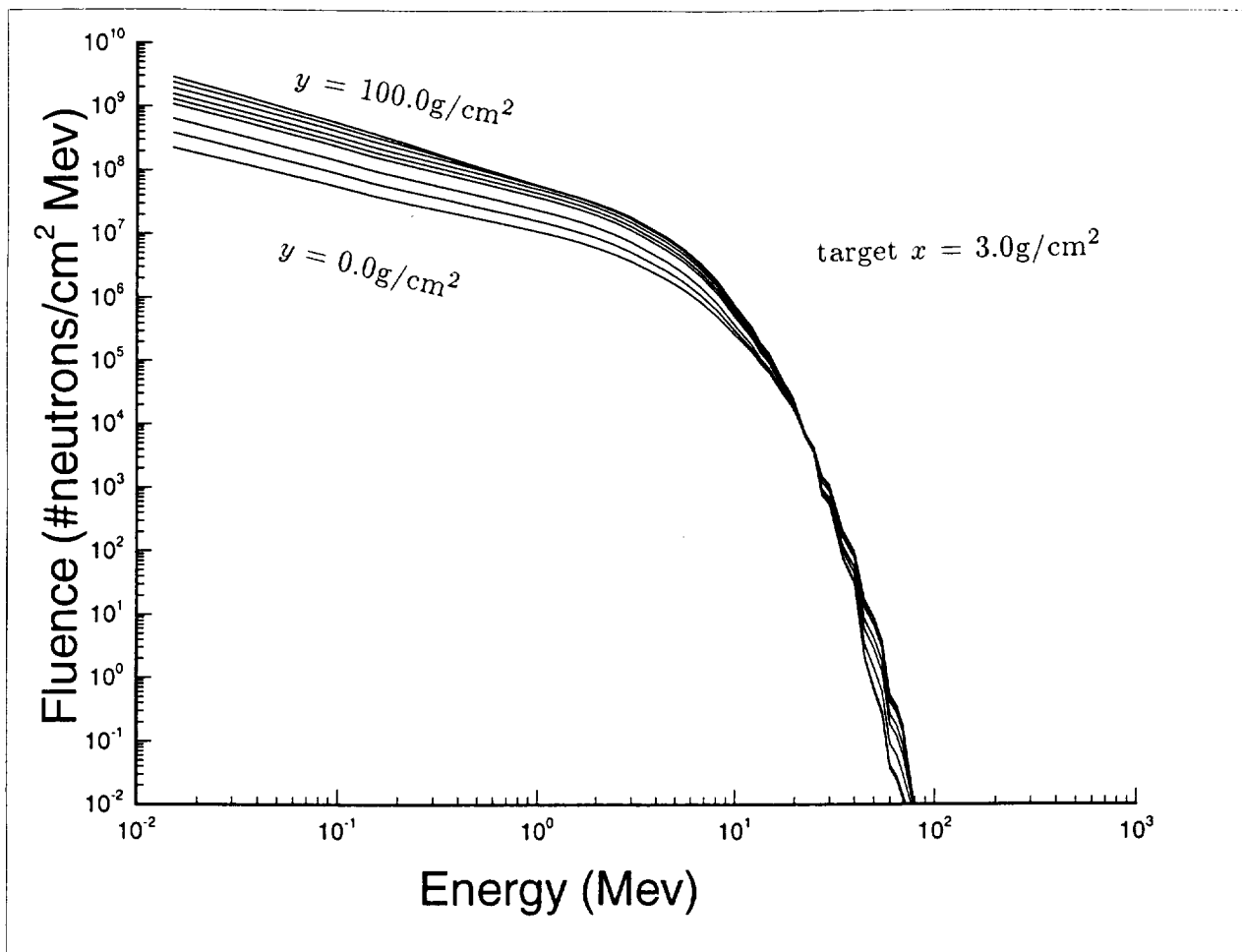
Figure 13. Multi-group low energy evaporation neutron fluence vs energy for target 3.0 g/cm^2 and various shield thicknesses.
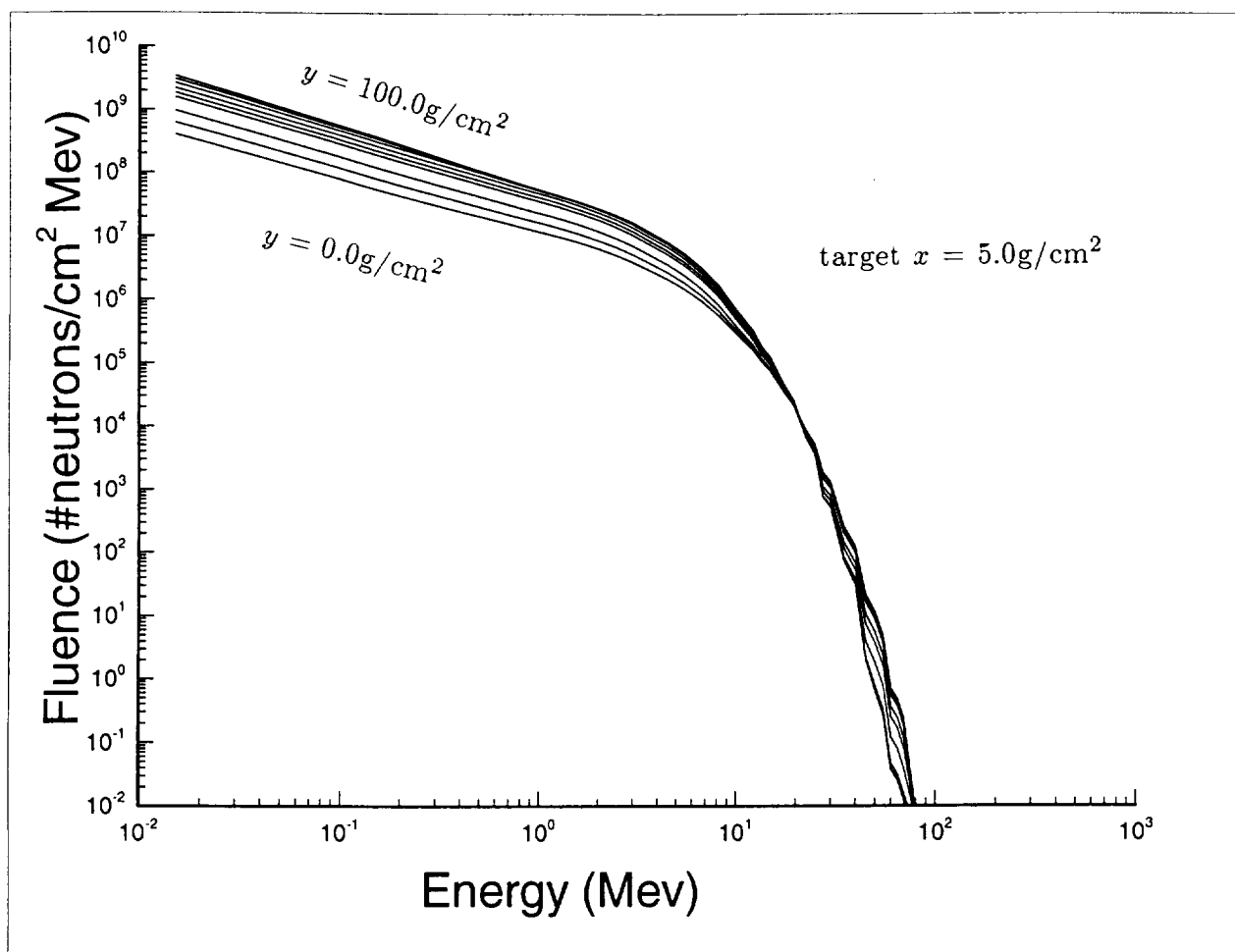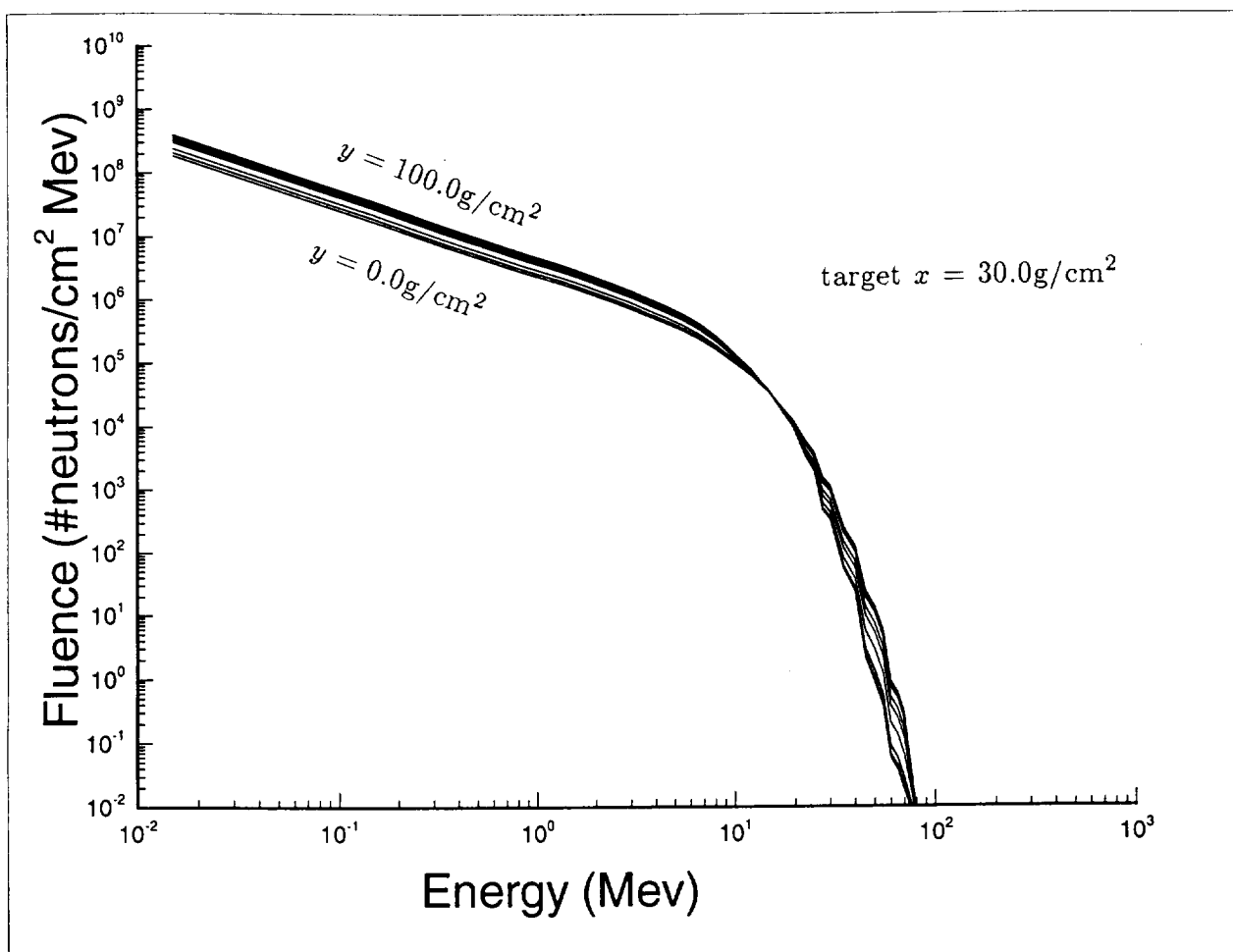
Figure 14. Multi-group low energy evaporation neutron fluence vs energy for target 5.0 g/cm^2 and various shield thicknesses.

Figure 15. Multi-group low energy evaporation neutron fluence
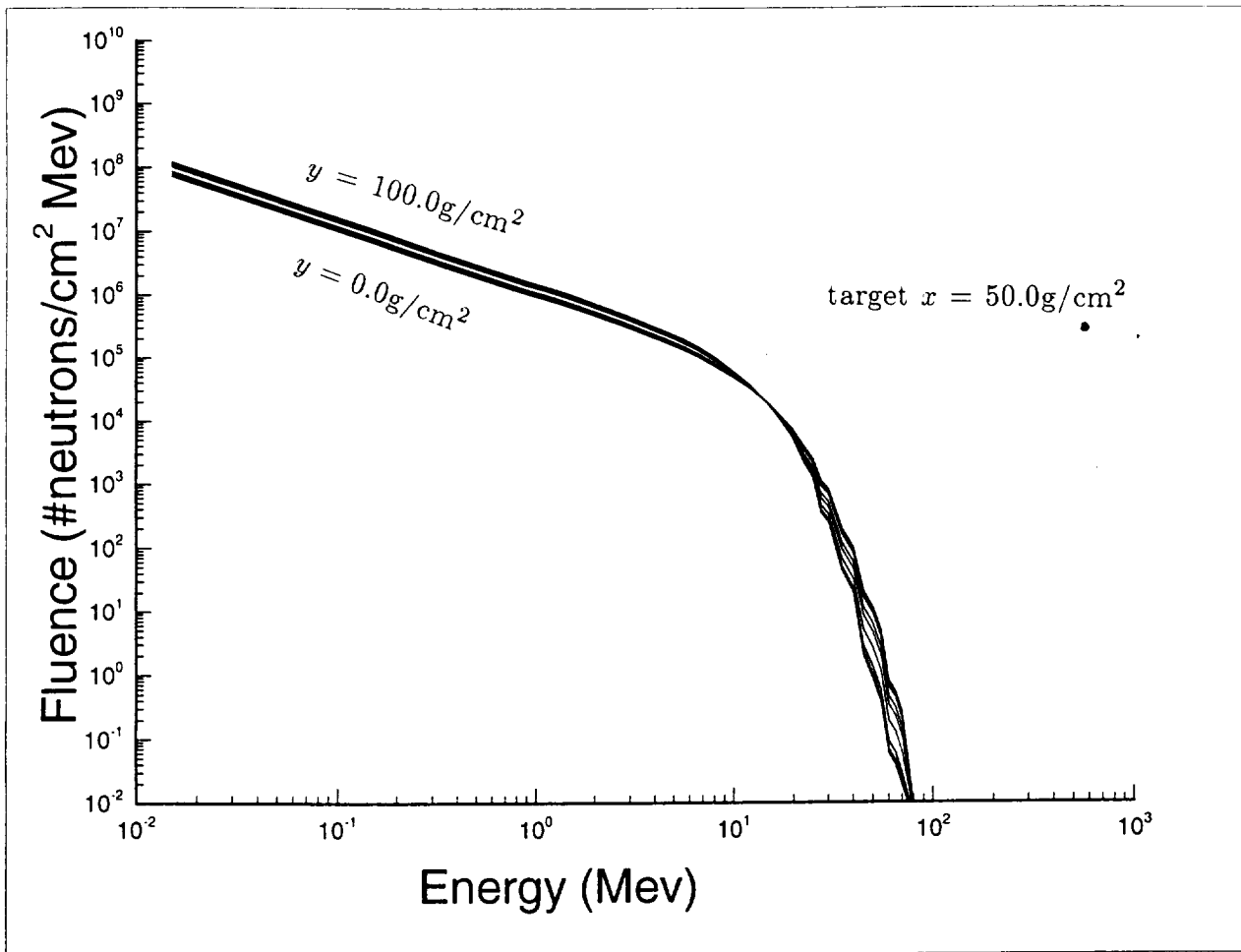vs energy for target 10.0 g/cm^2 and various shield thicknesses.

Figure 16. Multi-group low energy evaporation neutron fluence vs energy for target 20.0 g/cm^2 and various shield thicknesses.

Figure 17. Multi-group low energy evaporation neutron fluence
vs energy for target 30.0 g/cm^2 and various shield thicknesses.

Figure 18. Multi-group low energy evaporation neutron fluence
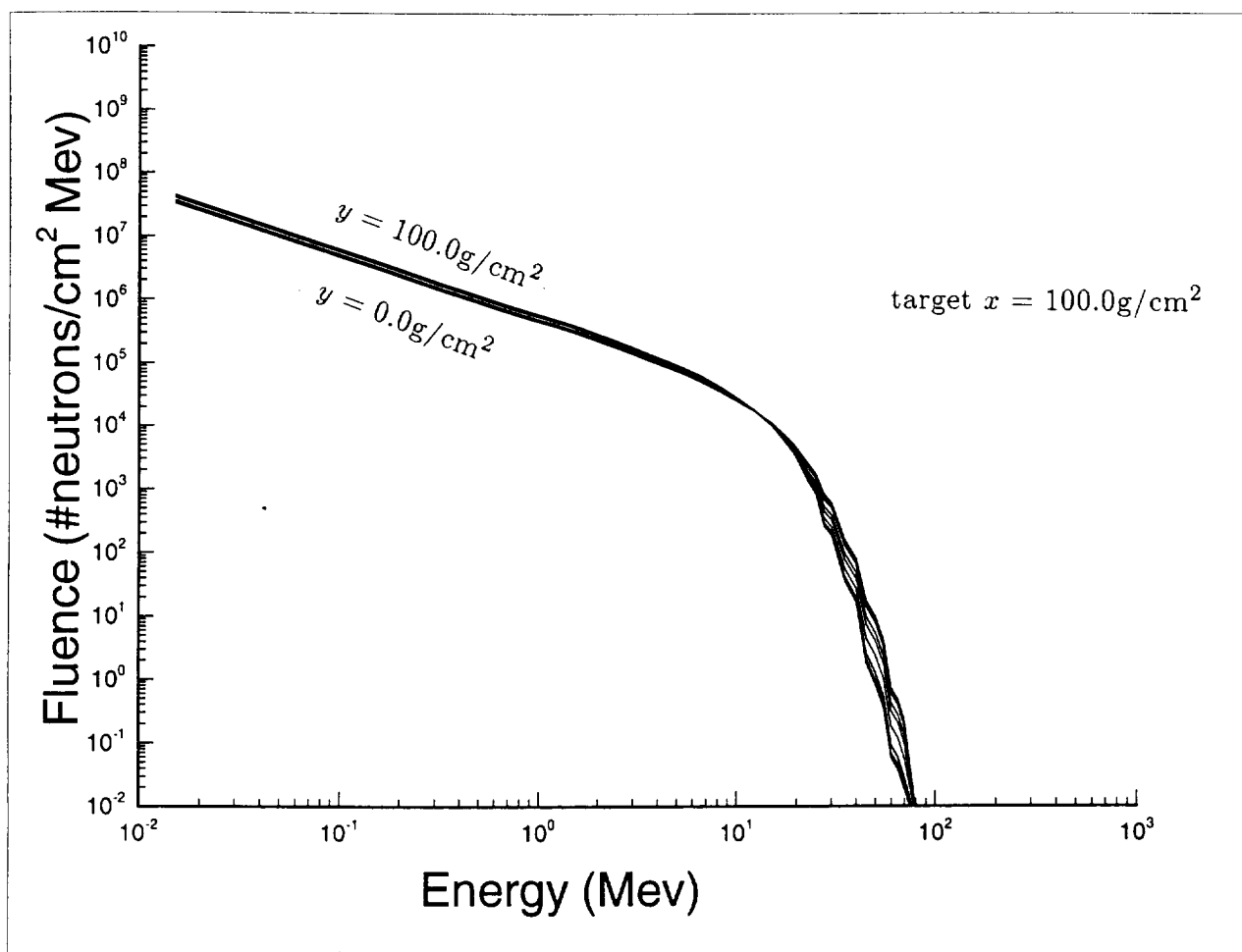vs energy for target 50.0 g/cm^2 and various shield thicknesses.

Figure 19. Multi-group low energy evaporation neutron fluence vs energy for target 100.0 g/cm^2 and various shield thicknesses.
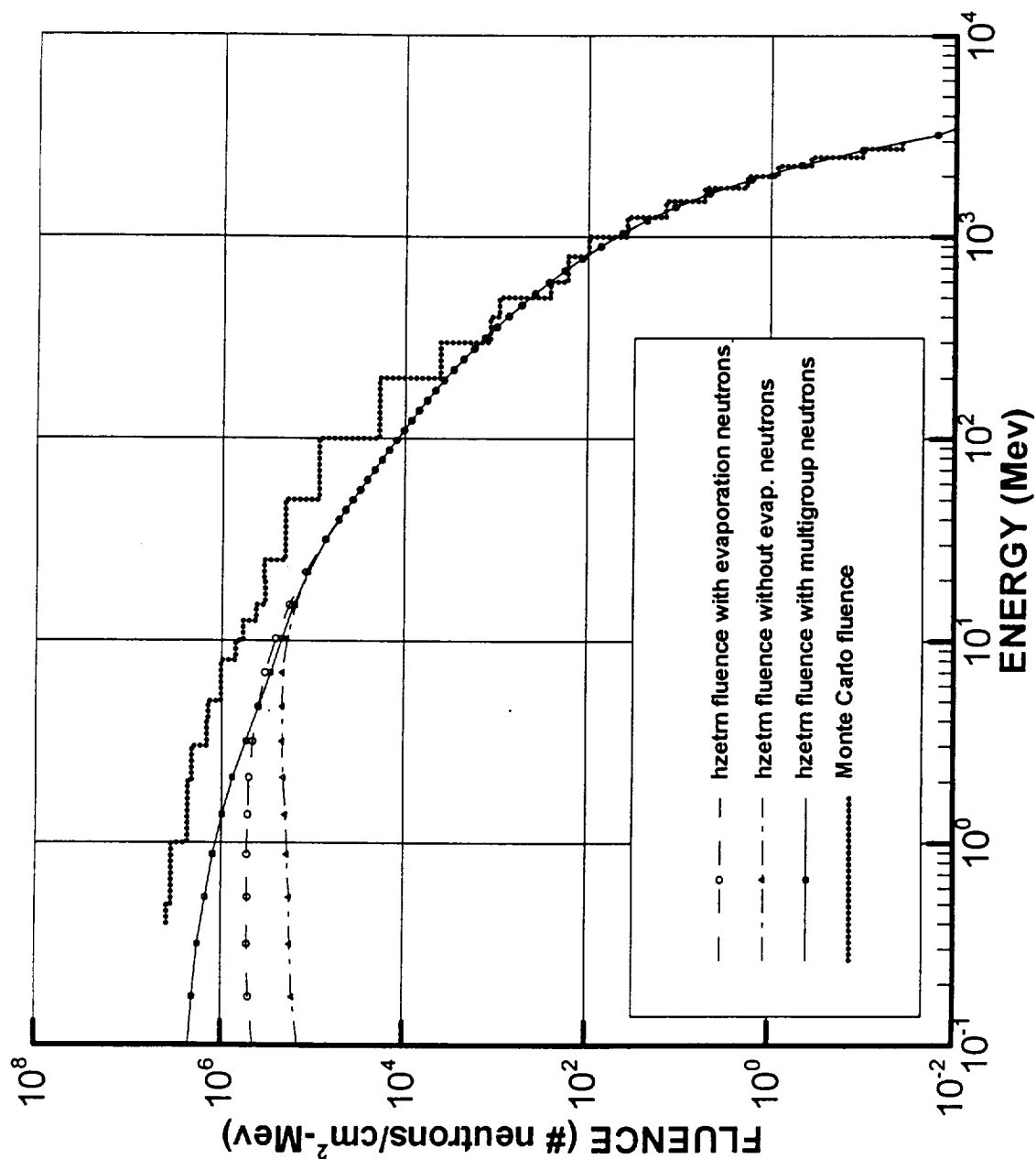
Figure 20. Energy spectra of neutron fluence at $1.0 g/cm^2$ depth of water slab exposed to February 1956 solar flare, as calculated by HZETRN with and without multi-group addition of low energy evaporation neutrons.

Figure 21. Energy spectra of neutron fluence at $10.0 g/cm^2$ depth of water slab exposed to February 1956 solar flare, as calculated by HZETRN with and without multi-group addition of low energy evaporation neutrons.

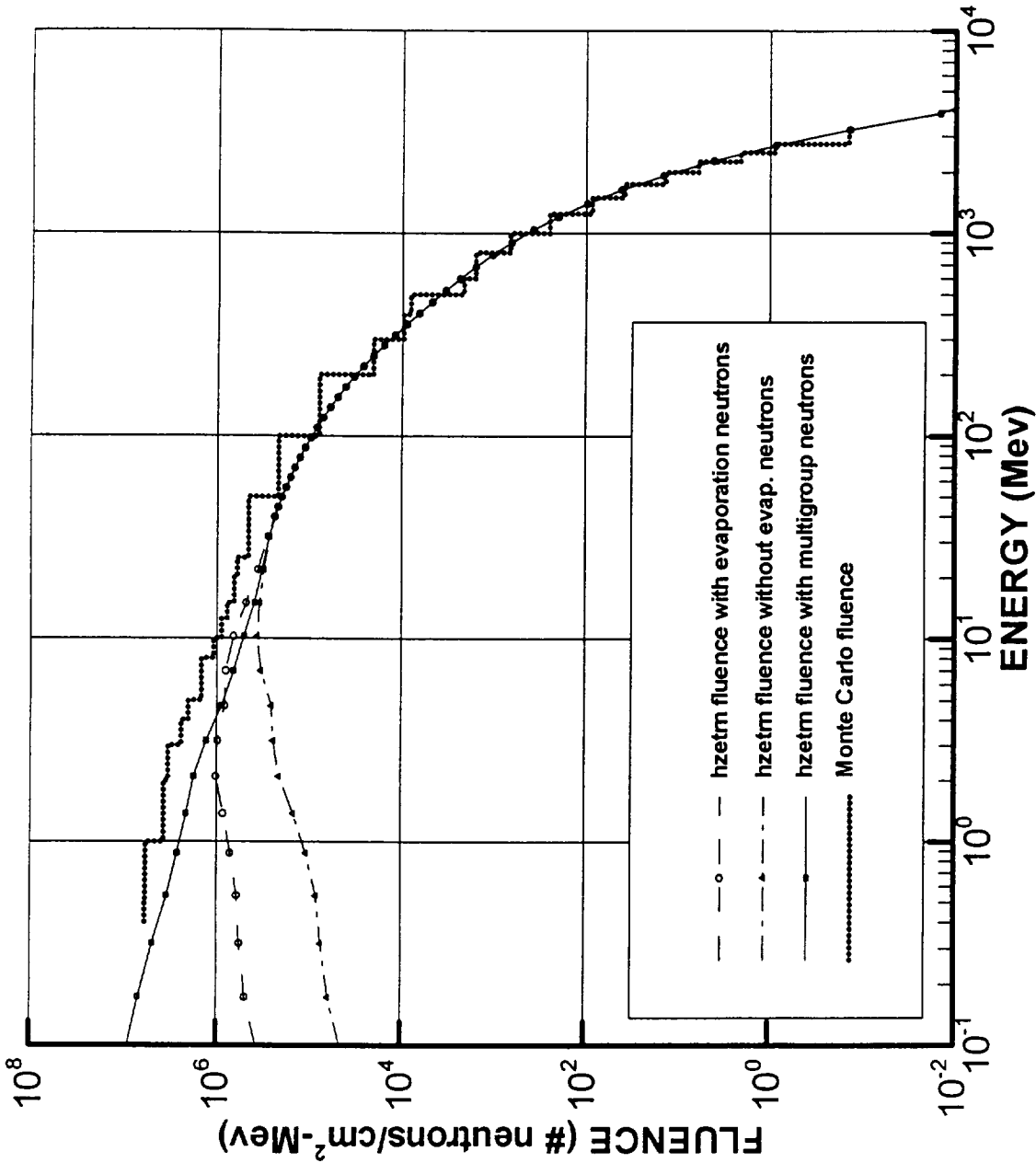NEUTRON FLUENCE FOR TARGET DEPTH 30 g/cm² OF WATER, NO SHIELD

Figure 22. Energy spectra of neutron fluence at $30.0 g/cm^2$ depth of water slab exposed to February 1956 solar flare, as calculated by HZETRN with and without multi-group addition of low energy evaporation neutrons.
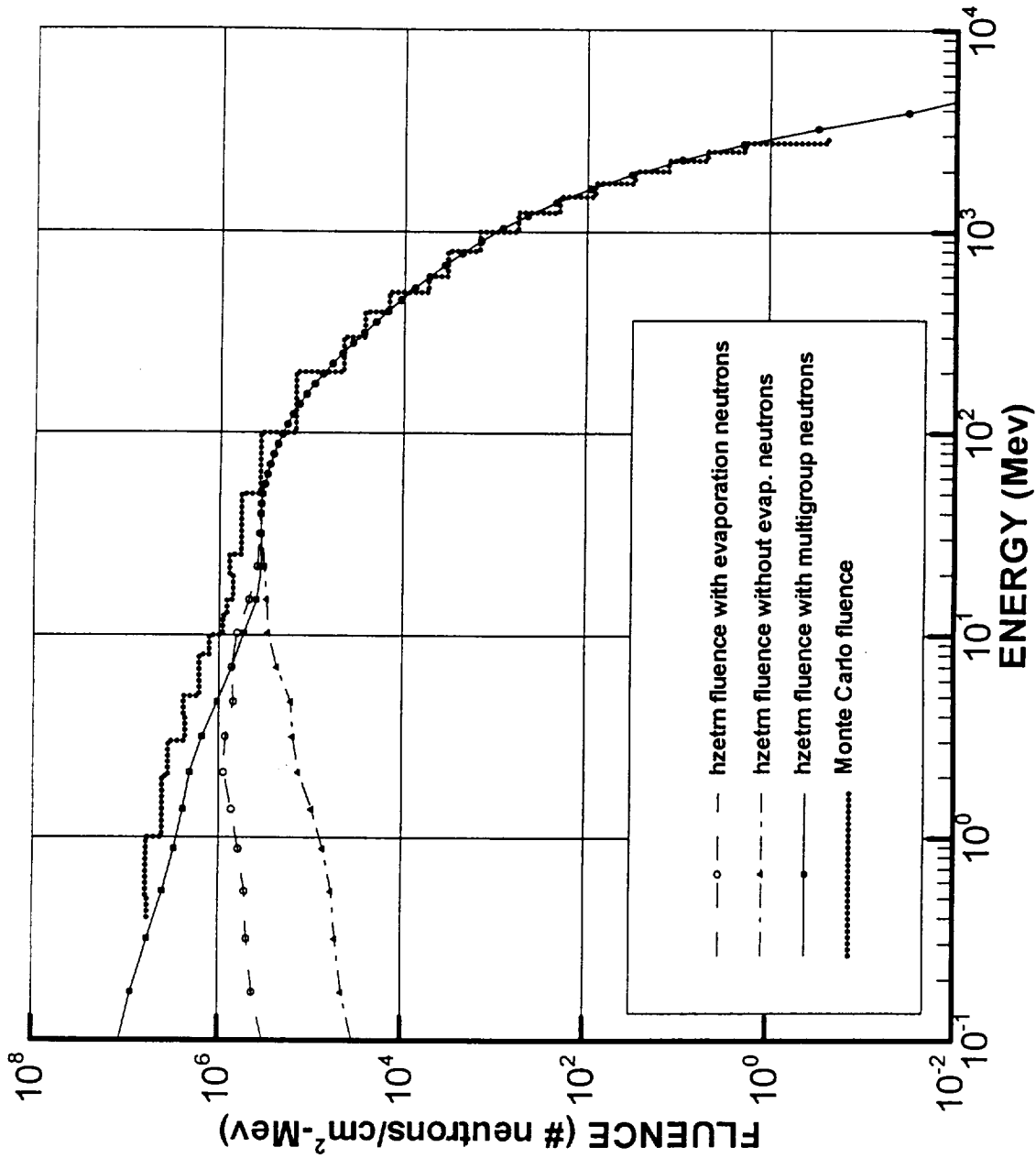
Appendix C

Green's Function Associated with the Transport of Light Ions in Matter.

Green's Function Associated with the Transport of Light Ions in Matter.

Basic Boltzmann equation

$$
\begin{pmatrix}
\text{Change in ion flux} \\
\text{within a volume element}
\end{pmatrix}
=
\begin{pmatrix}
\text{Gains within the} \\
\text{volume element}
\end{pmatrix}
-
\begin{pmatrix}
\text{Losses due to any} \\
\text{nuclear collisions}
\end{pmatrix}
$$

This gives the Boltzmann equation

$$
\left[\vec{\Omega} \cdot \nabla - \frac{1}{A_j} \frac{\partial}{\partial E} S_j(E) + \sigma_j(E) \right] \phi_j(\vec{x}, \vec{\Omega}, E) = \sum_{k>j} \int_E^\infty dE' \int d\vec{\Omega}' r_{jk} \phi_k(\vec{x}, \vec{\Omega}', E') \quad (1)
$$

where

$\phi_j(\vec{x}, \vec{\Omega}, E)$ is the flux of ions of type j moving in direction $\vec{\Omega}$

         having units ($\#\text{particles}/\text{cm}^2 - \sec - \text{sr} - \text{Mev}/\text{amu}$)

E is the ion energy. (Mev/amu)

A_j is the atomic mass of the jth type ion (amu)

$\sigma_j(E)$ is the macroscopic cross section. (cm^{-1})

$S_j(E)$ is the average energy loss per unit length or stopping power

         or linear energy transfer $\frac{dE}{dx}$. (Mev/cm).

$R_j(E)$ is the slowing down range for type j ions.   (cm) $R_j(E) = \int_0^E \frac{A_j \, dE'}{S_j(E')}$

j is the ion type.

$\vec{\Omega}$ is a unit vector in the direction of propagation.

r_{jk} is production cross section of type j ions with energy E and direction $\vec{\Omega}$

         by collision with type k ions of energy E' and direction $\vec{\Omega}'$

         having units of ($\text{cm} - \text{sr} - \text{Mev}/\text{amu}$)

$\hat{n}$ is the outward directed unit normal to boundary.

$\vec{\Gamma}$ is vector to boundary point. (cm)

$\vec{x}$ is the position vector to arbitray point in region (cm) $\vec{x} = \rho \vec{\Omega} + \vec{x}_n$

ρ is the projection of $\vec{x}$ on $\vec{\Omega}$ (cm)

$\vec{x}_n$ is the component of $\vec{x}$ perpendicular to $\vec{\Omega}$ direction.

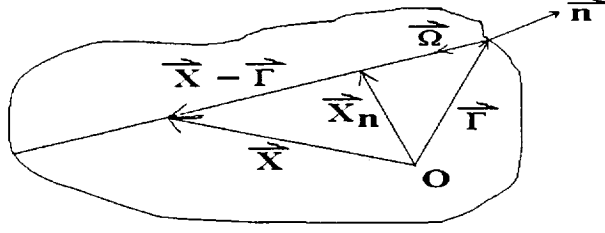The equation (1) is to be associated with the geometry of figure 1.

Figure 1. General Geometry for Boltzmann's equation

Multiply the equation (1) by $S_j(E)$ and define the quantities

$$\overline{\phi}_j(\vec{x}, \vec{\Omega}, E) = S_j(E)\phi_j(\vec{x}, \vec{\Omega}, E) \tag{2}$$

$$\overline{G}_j(\vec{x}, \vec{\Omega}, E) = S_j(E) \sum_{k>j} \int_E^\infty dE' \int d\vec{\Omega}' \, r_{jk}\phi_k(\vec{x}, \vec{\Omega}', E') \tag{3}$$

to obtain

$$\left[\vec{\Omega} \cdot \nabla - \frac{S_j(E)}{A_j} \frac{\partial}{\partial E} + \sigma(E)\right] \overline{\phi}_j(\vec{x}, \vec{\Omega}, E) = \overline{G}_j(\vec{x}, \vec{\Omega}, E). \tag{4}$$

Note that $\vec{\Omega} \cdot \nabla \overline{\phi}_j = \frac{\partial \overline{\phi}_j}{\partial \rho}$ is the directional derivative in the direction $\vec{\Omega}$ and that

$$\frac{\partial \overline{\phi}_j}{\partial E} = \frac{\partial \overline{\phi}_j}{\partial R_j} \frac{\partial R_j}{\partial E} = \frac{\partial \overline{\phi}_j}{\partial R_j} \frac{A_j}{S_j(E)}$$

so that the equation (4) can be written as

$$\left[\frac{\partial}{\partial \rho} - \frac{\partial}{\partial R_j} + \sigma(E)\right] \overline{\phi}_j(\vec{x}, \vec{\Omega}, E) = \overline{G}_j(\vec{x}, \vec{\Omega}, E). \tag{5}$$

Introduce the characteristic variables (η_j, ξ_j) given by the transformation equations

$$\eta_j = \rho - R_j(E) \qquad \xi_j = \rho + R_j(E) \tag{6}$$

59

where $\rho = \vec{\Omega} \cdot \vec{x}$. Also introduce the variables

$$\chi_j(\eta_j, \xi_j) = \overline{\phi}_j(\rho\vec{\Omega} + \vec{x}_n, \vec{\Omega}, E)$$

$$g_j(\eta_j, \xi_j) = \overline{G}_j(\rho\vec{\Omega} + \vec{x}_n, \vec{\Omega}, E) \tag{7}$$

$$\overline{\sigma}_j(\eta_j, \xi_j) = \sigma_j(E)$$
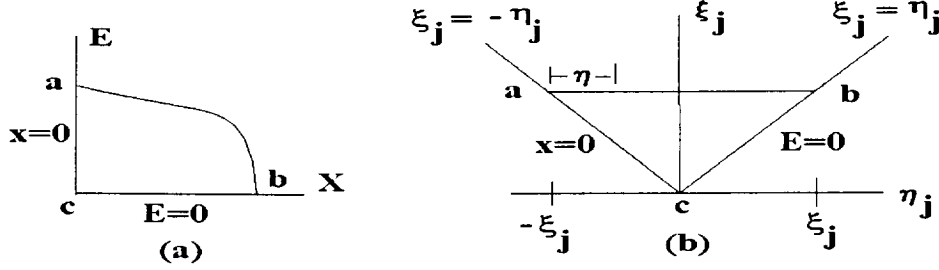

Figure 2. Geometry for characteristic variables

By the chain rule we have

$$\frac{\partial \overline{\phi}_j}{\partial \rho} = \frac{\partial \overline{\phi}}{\partial \eta_j} + \frac{\partial \overline{\phi}_j}{\partial \xi_j} \quad \text{and} \quad \frac{\partial \overline{\phi}_j}{\partial R_j} = \frac{\partial \overline{\phi}}{\partial \eta_j}(-1) + \frac{\partial \overline{\phi}_j}{\partial \xi_j}$$

so that the equation (5) simplifies to

$$\left(2\frac{\partial}{\partial \eta_j} + \overline{\sigma}_j\right)\chi_j(\eta_j, \xi_j) = g_j(\eta_j, \xi_j) \tag{8}$$

in terms of the new variables. This equation can be integrated using the integrating factor

$$\exp\left[\frac{1}{2}\int_a^{\eta_j} \overline{\sigma}_j(\eta', \xi_j)\, d\eta'\right] \tag{9}$$

to obtain

$$\chi_j(\eta_j, \xi_j) = \exp[-\frac{1}{2}\int_a^{\eta_j} \overline{\sigma}_j(\eta', \xi_j)d\eta']\chi_j(a, \xi_j)$$

$$+ \frac{1}{2}\int_a^{\eta_j} \exp[-\frac{1}{2}\int_{\eta'}^{\eta_j} \overline{\sigma}(\eta'', \xi_j)\, d\eta'']g_j(\eta', \xi_j)\, d\eta' \tag{10}$$

60

where a is any real number. Consequently, the solution to the equation (4) can be written as

$$\overline{\phi}_j(\vec{x}, \vec{\Omega}, E) = f(a, \rho - R_j(E))\overline{\phi}_j \left(\frac{1}{2}(\xi_j + a)\vec{\Omega} + \vec{x}_n, \vec{\Omega}, R_j^{-1}(\frac{\xi_j - a}{2}) \right)$$
$$+ \frac{1}{2} \int_a^{\rho - R_j(E)} f(\eta'', \rho - R_j(E))\overline{G}_j \left(\frac{1}{2}(\xi_j + \eta'')\vec{\Omega} + \vec{x}_n, \vec{\Omega}, R_j^{-1}(\frac{\xi_j - \eta''}{2}) \right) d\eta'' \qquad (11)$$

where

$$f(a, \rho - R_j(E)) = \exp\left[-\frac{1}{2} \int_a^{\rho - R_j(E)} \sigma_j(R_j^{-1}(\frac{\xi_j - \eta'}{2})) \, d\eta' \right] \qquad (12)$$

From equations (6) we find that

$$2\rho = \eta_j + \xi_j \quad \text{and} \quad 2R_j(E) = \xi_j - \eta_j \qquad (13)$$

so that when $\eta' = a$ we will have $\rho = \frac{1}{2}(a + \xi_j)$. Observe from figure 2 that along the line of integration we will have $\xi_j = $ constant. The value of a is selected such that $\rho\vec{\Omega} + \vec{x}_n = \vec{\Gamma}$ is a point on the boundary. Thus, the vector $\left(\frac{a + \xi_j}{2} \right) \vec{\Omega} + \vec{x}_n = \vec{\Gamma}$ dotted with $\vec{\Omega}$ gives the value

$$a = 2\vec{\Omega} \cdot \vec{\Gamma} - \xi_j = 2d - \rho - R_j(E) \qquad (14)$$

where $d = \vec{\Omega} \cdot \vec{\Gamma}$. Note that when $E = E'$ and $\eta_j = \eta'$ we have from equation (13) that

$$2R_j(E') = \xi_j - \eta' \qquad (15)$$

or

$$E' = R_j^{-1}\left(\frac{\xi_j - \eta'}{2} \right) = R_j^{-1}\left(\frac{\rho + R_j(E) - \eta'}{2} \right) \quad \text{with} \quad dE' = \frac{-S_j(E')}{2A_j} \, d\eta' \qquad (16)$$

and similarly by changing symbols when

$$E'' = R_j^{-1}\left(\frac{\rho + R_j(E) - \eta''}{2} \right) \quad \text{we have} \quad dE'' = \frac{-S_j(E'')}{2A_j} \, d\eta''. \qquad (17)$$

We examine the limits of integration in equation (11) and observe that when $\eta' = a$ we have

$$2R_j(E') = \rho + R_j(E) - a \qquad (18)$$

and from equation (14) we have

$$2d = \rho + R_j(E) + a. \qquad (19)$$

61

Adding the equations (18) and (19) we find

$$R_j(E') + d = \rho + R_j(E) \tag{20}$$

or

$$E' = R_j^{-1}(\rho - d + R_j(E)). \tag{21}$$

Next we examine the lower limit of integration and find that when $\eta' = \rho - R_j(E)$, then $2R_j(E') = \rho + R_j(E) - \rho + R_j(E)$ implies that $E' = E$. In the second term of equation (11) when $\eta'' = a$ we again find that $E'' = R_j^{-1}(\rho + R_j(E) - d)$ and when $\eta'' = \rho - R_j(E)$ then $E'' = E$. Also,

$$\frac{1}{2}(\xi_j + \eta'') = \frac{1}{2}(\xi_j + \xi_j - 2R_j(E'')) = \xi_j - R_j(E'') = \rho + R_j(E) - R_j(E'').$$

Consequently, the equation (11) can be written in the form

$$\begin{aligned}
\overline{\phi}_j(\vec{x}, \vec{\Omega}, E) &= F_1(E, R_j^{-1}(R_j(E) - d + \rho)\overline{\phi}_j(\vec{\Gamma}, \vec{\Omega}, R_j^{-1}(R_j(E) + \rho - d)) \\
&+ \int_E^{R_j^{-1}(R_j(E) + \rho - d)} F_1(E, E'')\overline{G}_j((\rho + R_j(E) - R_j(E''))\vec{\Omega} + \vec{x}_n, \vec{\Omega}, E'')\frac{A_j}{S_j(E'')} dE''
\end{aligned} \tag{22}$$

where

$$F_1(E1, E2) = \exp\left[-\int_{E1}^{E2} \frac{A_j\sigma_j(E')}{S_j(E')} dE'\right] \tag{23}$$

Define the nuclear survival probability (reference Wilson 1977) as

$$P_j(E) = \exp\left[-\int_0^E \frac{A_j\sigma_j(E')}{S_j(E')} dE'\right] \tag{24}$$

then the equation (23) can be written as

$$F_1(E_1, E_2) = \frac{P_j(E_2)}{P_j(E_1)}.$$

Then from equation (22) we can write the solution to equation (3) in the form

$$\begin{aligned}
\phi_j(\vec{x}, \vec{\Omega}, E) &= \frac{S_j(E_j)P_j(E_j)}{S_j(E)P_j(E)}\phi_j(\vec{\Gamma}, \vec{\Omega}, E_j) \\
&+ \sum_{k>j} \int_E^{E_j} dE' \frac{A_j P_j(E')}{S_j(E)P_j(E)} \int_{E'}^{\infty} dE'' \int d\vec{\Omega}' r_{jk}(E', E'')\phi_k(\vec{x} + (R_j(E) - R_j(E'))\vec{\Omega}, \vec{\Omega}', E'')
\end{aligned} \tag{25}$$

where $E_j = R_j^{-1}(\rho + R_j(E) - d)$, $\vec{x} = \vec{x}_n + \rho\vec{\Omega}$ and E' and E'' have been interchanged.

62

In the one-dimensional straight ahead approximation $\vec{\Omega}$ is a unit vector in the direction of $\vec{x}$ with $\rho = x$, $\vec{x}_n = \vec{0}$, $\eta_j = x - R_j(E)$, $\xi_j = x + R_j(E)$ and $\vec{\Gamma} = \vec{0}$. (i.e. the origin 0 moves to the boundary $x = 0$). The equation (25) then reduces to

$$
\begin{aligned}
\phi_j(x, E) = {} & \frac{S_j(E_j)P_j(E_j)}{S_j(E)P_j(E)}\, \phi_j(0, E_j) \\
& + \sum_{k>j} \int_E^{E_j} dE'\, \frac{A_j P_j(E')}{S_j(E)P_j(E)} \int_{E'}^{\infty} dE''\, \sigma_{jk}(E', E'')\phi_k(x + R_j(E) - R_j(E'), E'')
\end{aligned}
\tag{26}
$$

where E_j is determined from x and E such that

$$
E_j = R_j^{-1}(x + R_j(E)).
\tag{27}
$$

The solution given by equation (26) can be expressed in terms of Green's function as

$$
\phi_j(x, E) = \sum_{k>j} \int_0^{\infty} G_{jk}(x, E, E_0)\phi_k(0, E_0)\, dE_0
\tag{28}
$$

where $\phi_k(0, E_0) = f_k(E_0)$ are boundary conditions. Substituting the assumed solution given by equation (28) into equation (26) we obtain

$$
\begin{aligned}
\sum_{\ell} \int_0^{\infty} G_{j\ell}(x, E, E_0)\phi_\ell(0, E_0)dE_0 = {} & \sum_{\ell} \int_0^{\infty} \frac{S_j(E_j)P_j(E_j)}{S_j(E)P_j(E)} G_{j\ell}(0, E_j, E_0)\phi_\ell(0, E_0)dE_0 \\
& + \sum_k \int_E^{E_j} dE'\, \frac{A_j P_j(E')}{S_j(E)P_j(E)} \int_{E'}^{\infty} dE'' \sigma_{jk}(E', E'') \sum_{\ell} \int_0^{\infty} G_{k\ell}(x + R_j(E) - R_j(E'), E'', E_0)\phi_\ell(0, E_0)\, dE_0.
\end{aligned}
$$

Note that when $\ell = m$ we can equate like coefficients and find that $G_{jm}(x, E, E_0)$ must satisfy the integral equation

$$
\begin{aligned}
G_{jm}(x, E, E_0) = {} & \frac{S_j(E_j)P_j(E_j)}{S_j(E)P_j(E)}\, G_{jm}(0, E_j, E_0) \\
& + \sum_{k>j} \int_E^{E_j} dE'\, \frac{A_j P_j(E')}{S_j(E)P_j(E)} \int_{E'}^{\infty} dE''\, \sigma_{jk}(E', E'')G_{km}(x + R_j(E) - R_j(E'), E'', E_0)
\end{aligned}
\tag{29}
$$

subject to the boundary condition $G_{jm}(0, E, E_0) = \delta_{jm}\delta(E - E_0)$, where the value for E_j is determined from the inverse relation $E_j = R_j^{-1}(x + R_j(E))$. The G_{jm} terms are written using the Neumann expansion as a perturbation series

$$
G_{jm}(x, E, E_0) = \sum_{i=0}^{\infty} G_{jm}^{(i)}(x, E, E_0)
\tag{30}
$$

63

with leading term

$$G_{jm}^{(0)}(x, E, E_0) = \frac{S_j(E_j)P_j(E_j)}{S_j(E)P_j(E)}\delta_{jm}\delta(E_j - E_0).$$ (31)

with $E_j = R_j^{-1}(x + R_j(E))$. Note that when $x = 0$ we have $E_j = E$ so that $G_{jm}^{(0)}(0, E, E_0)$ satisfies the above boundary condition. The higher order terms are determined from the recursive definition

$$G_{jm}^{(n+1)}(x, E, E_0) =$$
$$\sum_k \int_E^{E_j} dE' \frac{A_j P_j(E')}{S_j(E)P_j(E)} \int_{E'}^{\infty} dE'' \sigma_{jk}(E', E'')G_{km}^{(n)}(x + R_j(E) - R_j(E'), E'', E_0).$$ (32)

and must satisfy the boundary conditions $G_{jm}^{(n+1)}(x, E, E_0) = 0$ for $n = 0, 1, 2, \ldots$. In the special case $n = 0$ the equation (32) reduces to

$$G_{jm}^{(1)}(x, E, E_0) =$$
$$\sum_k \int_E^{E_j} dE' \frac{A_j P_j(E')}{S_j(E)P_j(E)} \int_{E'}^{\infty} dE'' \sigma_{jk}(E', E'') \frac{S_k(E_k')P_k(E_k')}{S_k(E'')P_k(E'')}\delta_{km}\delta(E_k' - E_0)$$ (33)

where $R_k(E_k') = x + R_j(E) - R_j(E') + R_k(E'')$. (i.e. treat $x + R_j(E) - R_j(E'')$ as an x^* value. See for example equation (27) .) Again we observe that when $x = 0$ we have $E_j = E$ and so the boundary condition at $x = 0$ is satisfied.

Cross Section assumption 1

For interactions dominated by perpherial processes we use

$$\sigma_{jm}(E', E'') = \sigma_{jm}(E'')\delta(E' - E'')$$ (34)

so that the equation (33) becomes

$$G_{jm}^{(1)}(x, E, E_0) =$$
$$\sum_k \int_E^{E_j} dE' \frac{A_j P_j(E')}{S_j(E)P_j(E)} \int_{E'}^{\infty} dE'' \sigma_{jk}(E'')\delta(E' - E'') \frac{S_k(E_k')P_k(E_k')}{S_k(E'')P_k(E'')}\delta_{km}\delta(E_k' - E_0)$$ (35)

where

$$E_k' = R_k^{-1}(x + R_j(E) - R_j(E') + R_k(E'')).$$ (36)

We integrate with respect to E'' and observe that the only nonzero term occurs when $E'' = E'$. This gives

$$G_{jm}^{(1)}(x, E, E_0) = \sum_k \int_E^{E_j} dE' \frac{A_j P_j(E')}{S_j(E)P_j(E)}\sigma_{jk}(E') \frac{S_k(E_k')P_k(E_k')}{S_k(E')P_k(E')}\delta(E_k' - E_0)\delta_{km}$$ (37)

64

where

$$R_k(E_k') = x + R_j(E) - R_j(E') + R_k(E') \tag{38}$$

$$R_j(E') - R_k(E') = x + R_j(E) - R_k(E_k').$$

We know that $\nu_j R_j(E') = \nu_k R_k(E')$ so that the above can be written as

$$\left(\frac{\nu_k}{\nu_j} - 1\right) R_k(E') = x + R_j(E) - R_k(E_k')$$

$$\text{or} \quad \left(1 - \frac{\nu_j}{\nu_k}\right) R_j(E') = x + R_j(E) - R_k(E_k')$$

Thus, we can write

$$R_j(E') = \frac{\nu_k}{|\nu_k - \nu_j|}(x + R_j(E) - R_k(E_k'))$$

$$\text{or} \quad R_k(E') = \frac{\nu_j}{|\nu_k - \nu_j|}(x + R_j(E) - R_k(E_k')). \tag{39}$$

Differentiate the equation (39) with respect to E_k' to obtain

$$R_k'(E')dE' = \frac{\nu_j}{|\nu_k - \nu_j|}(-R_k'(E_k'))dE_k' \quad \text{or} \quad dE' = \frac{\nu_j}{|\nu_k - \nu_j|}\frac{\frac{A_k}{S_k(E_k')}}{\frac{A_k}{S_k(E')}}dE_k' \tag{40}$$

The equation (35) can then be written as

$$G_{jm}^{(1)}(x, E, E_0) = \sum_k \int_{E_{k1}'}^{E_{k2}'} dE_k' \frac{A_j P_j(E')}{S_j(E)P_j(E)}\sigma_{jk}(E')\frac{\nu_j}{|\nu_k - \nu_j|}\frac{P_k(E_k')}{P_k(E')}\delta(E_k' - E_0)\delta_{km} \tag{41}$$

The only nonzero contribution comes when $k = m$ and $E_k' = E_0$ and so equation (41) reduces to

$$G_{jm}^{(1)}(x, E, E_0) = \begin{cases} h_{jm}(x, E, E_0, E') & \text{if } \frac{\nu_m}{\nu_j}(R_m(E_0) - x) < R_j(E) < \frac{\nu_m}{\nu_j}R_m(E_0) - x \\ 0 & \text{otherwise} \end{cases} \tag{42}$$

where

$$h_{jm}(x, E, E_0, E') = \frac{A_j P_j(E')}{S_j(E)P_j(E)}\sigma_{jm}(E')\frac{\nu_j}{|\nu_m - \nu_j|}\frac{P_m(E_0)}{P_m(E')} \tag{43}$$

and

$$E' = R_j^{-1}\left(\frac{\nu_m}{|\nu_m - \nu_j|}[x + R_j(E) - R_m(E_0)]\right). \tag{44}$$

That is, when $E'_k = E_0$ and $k = m$ we have from the equation (38) that

$$R_m(E_0) = x + R_j(E) - R_j(E') + R_m(E')$$

$$R_j(E') - R_m(E') = x + R_j(E) - R_m(E_0)$$

$$\left(1 - \frac{\nu_j}{\nu_m}\right) R_j(E') = x + R_j(E) - R_m(E_0)$$

$$R_j(E') = \frac{\nu_m}{|\nu_m - \nu_j|}(x + R_j(E) - R_m(E_0)).$$

Also from the transformation equations (13) the $\eta_k, \xi_k, \eta_j, \xi_j$ variables are related through the range scale factors ν_j and ν_k, where $\nu_j R_j = \nu_k R_k$. This produces the relations

$$\eta_k - \xi_k = -2R_k = -2\frac{\nu_j}{\nu_k}R_j = \frac{\nu_j}{\nu_k}(\eta_j - \xi_j).$$

Then from the equations

$$\xi_j + \eta_j = \xi_k + \eta_k \tag{45}$$

$$\eta_j - \xi_j = \frac{\nu_k}{\nu_j}(\eta_k - \xi_k) \tag{46}$$

we find that by adding the equation (45) and (46) we obtain

$$2\eta_j = \left(1 + \frac{\nu_k}{\nu_j}\right)\eta_k + \left(1 - \frac{\nu_k}{\nu_j}\right)\xi_k \tag{47}$$

and subtracting (46) from (45) we obtain

$$2\xi_j = \left(1 - \frac{\nu_k}{\nu_j}\right)\eta_k + \left(1 + \frac{\nu_k}{\nu_j}\right)\xi_k. \tag{48}$$

Interchanging j and k in the equations (47) and (48) we find that

$$\eta_k = \left(\frac{\nu_j + \nu_k}{2\nu_k}\right)\eta_j + \left(\frac{\nu_k - \nu_j}{2\nu_k}\right)\xi_j$$

$$\xi_k = \left(\frac{\nu_k - \nu_j}{2\nu_k}\right)\eta_j + \left(\frac{\nu_k + \nu_j}{2\nu_k}\right)\xi_j.$$

Then when η_j is a value η' lying between the constants $-\xi_j$ and $+\xi_j$, (See Figure 2(b)), we will have

$$\eta_k = \left(\frac{\nu_j + \nu_k}{2\nu_k}\right)\eta' + \left(\frac{\nu_k - \nu_j}{2\nu_k}\right)\xi_j$$

$$\xi_k = \left(\frac{\nu_k - \nu_j}{2\nu_k}\right)\eta' + \left(\frac{\nu_k + \nu_j}{2\nu_k}\right)\xi_j.$$

Changing k to m we find

$$\xi_m = \left(\frac{\nu_m - \nu_j}{2\nu_m}\right)\eta' + \left(\frac{\nu_m + \nu_j}{2\nu_m}\right)\xi_j.$$

Note that the boundary condition $G_{jm}(0, E, E_0) = \delta_{jm}\delta(E - E_0)$ can be written in the form

$$G_{jm}(0, E, E_0) = \delta_{jm}\delta(R_j^{-1}(\xi_j) - E_0) = \delta_{jm}\delta(\xi_j - R_j(E_0)) = \delta(\xi_m - R_m(E_0))$$

so that when $\xi_m = R_m(E_0)$ we have

$$\eta' = \frac{2\nu_m}{\nu_m - \nu_j}R_m(E_0) - \left(\frac{\nu_m + \nu_j}{\nu_m - \nu_j}\right)\xi_j. \tag{49}$$

Using the equations (6) and (49) we now calculate the inequality which occurs in the equation (42). From the equation (10), with $a = -\xi$, we have the inequality $-\xi_j < \eta' < \eta_j$ which implies

$$-\xi_j < \eta' < \eta_j$$

$$-x - R_j(E) < \frac{2\nu_m}{\nu_m - \nu_j}R_m(E_0) - \left(\frac{\nu_m + \nu_j}{\nu_m - \nu_j}\right)(x + R_j(E)) < x - R_j(E)$$

$$-x < \frac{2\nu_m}{\nu_m - \nu_j}R_m(E_0) + R_j(E) - \left(\frac{\nu_m + \nu_j}{\nu_m - \nu_j}\right)(x + R_j(E)) < x$$

$$\left(\frac{\nu_m + \nu_j}{\nu_m - \nu_j}\right)x - x < \frac{2\nu_m R_m(E_0)}{\nu_m - \nu_j} + \left(1 - \frac{\nu_m + \nu_j}{\nu_m - \nu_j}\right)R_j(E) < x + \left(\frac{\nu_m + \nu_j}{\nu_m - \nu_j}\right)x$$

$$\nu_j x < \nu_m R_m(E_0) - \nu_j R_j(E) < \nu_m x$$

$$-\nu_j x > \nu_j R_j(E) - \nu_m R_m(E_0) > -\nu_m x$$

$$\nu_m R_m(E_0) - \nu_j x > \nu_j R_j(E) > \nu_m R_m(E_0) - \nu_m x$$

$$\frac{\nu_m}{\nu_j}R_m(E_0) - x > R_j(E) > \frac{\nu_m}{\nu_j}\left(R_m(E_0) - x\right)$$

$$\frac{\nu_m}{\nu_j}\left(R_m(E_0) - x\right) < R_j(E) < \frac{\nu_m}{\nu_j}R_m(E_0) - x$$

Cross Section assumption 2

We start with equation (33) and assume $\sigma_{jm}(E', E'')$ has a Gaussian distribution of the form

$$\sigma_{jm}(E', E'') = \bar{\sigma}_{jm}(E'')\frac{1}{\Delta_{jm}\sqrt{2\pi}}\exp\left[-\frac{(E' - E'' - \epsilon_{jm})^2}{2\Delta_{jm}^2}\right]$$

67

we can then write the equation (33) in the form

$$G_{jm}^{(1)}(x, E, E_0) = \int_E^{E_j} dE' \int_{E'}^{\infty} dE'' F_{jk} \delta_{km} \tag{50}$$

where

$$F_{jk} = \frac{A_j P_j(E')}{S_j(E) P_j(E)} \sigma_{jk}(E', E'') \frac{S_k(E_k') P_k(E_k')}{S_k(E'') P_k(E'')} \delta(E_k' - E_0) \tag{51}$$

with

$$E_k' = R_k^{-1}(x + R_j(E) - R_j(E') + R_k(E'')) \tag{52}$$

The integration of (50) is over the region illustrated in the figure 3 in the limit as $T \to \infty$. In expanded form the equation (50) has the form

$$
\begin{aligned}
&G_{jm}^{(1)}(x, E, E_0) = \\
&\int_E^{E_j} dE' \int_{E'}^{\infty} dE'' \frac{A_j P_j(E')}{S_j(E) P_j(E)} \, \sigma_{jk} \, \frac{S_k(E_k') P_k(E_k')}{S_k(E'') P_k(E'')} \delta_{km} \delta(E_k' - E_0).
\end{aligned}
\tag{53}
$$

where

$$\sigma_{jk} = \bar{\sigma}_{jk}(E'') \frac{1}{\Delta_{jk}\sqrt{2\pi}} \exp\left[-\frac{(E' - E'' - \epsilon_{jk})^2}{2\Delta_{jk}^2} \right]$$
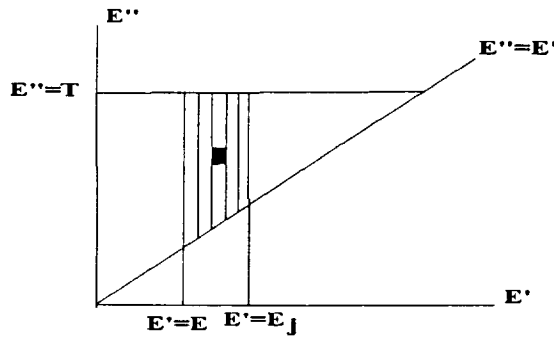

Figure 3. Limits of integration for Green's function term.

68

Note that for the first integration in the E'' direction we have E' is a constant. Consequently, we let

$$r = \frac{E'' + \epsilon_{jk} - E'}{\sqrt{2}\Delta_{jk}} \quad \text{with} \quad dr = \frac{dE''}{\sqrt{2}\Delta_{jk}} \tag{54}$$

The equation (53) can then be written in the form

$$G_{jm}^{(1)}(x, E, E_0) =$$
$$\int_E^{E_j} dE' \int_{\frac{\epsilon_{jk}}{\sqrt{2}\Delta_{jk}}}^{\infty} dr \frac{A_j P_j(E')}{\sqrt{\pi} S_j(E) P_j(E)} \bar{\sigma}_{jk}(\bar{r}) e^{-r^2} \frac{S_k(E_k') P_k(E_k')}{S_k(\bar{r}) P_k(\bar{r})} \delta_{km} \delta(E_k' - E_0). \tag{55}$$

where $\bar{r} = \sqrt{2}\Delta_{jk} r - \epsilon_{jk} + E'$ and

$$E_k' = R_k^{-1}(x + R_j(E) - R_j(E') - R_k(\bar{r})). \tag{56}$$

This integral can be simplified by using one of the mean value theorems for integrals and written as

$$G_{jm}^{(1)}(x, E, E_0) =$$
$$\int_E^{E_j} dE' \frac{A_j P_j(E')}{2 S_j(E) P_j(E)} \bar{\sigma}_{jk}(\bar{r}_*) \frac{S_k(E_{k_*}') P_k(E_{k_*}')}{S_k(\bar{r}_*) P_k(\bar{r}_*)} \delta_{km} \delta(E_{k_*}' - E_0) \frac{2}{\sqrt{\pi}} \int_{\frac{\epsilon_{jk}}{\sqrt{2}\Delta_{jk}}}^{\infty} e^{-r^2} dr. \tag{57}$$

with $\bar{r}_* = \sqrt{2}\Delta_{jk} r^* - \epsilon_{jk} + E'$ and

$$E_{k_*}' = R_k^{-1}(x + R_j(E) - R_j(E') - R_k(\bar{r}_*)) \tag{58}$$

where r^* is some mean value in the interval $(\frac{\epsilon_{jk}}{\sqrt{2}\Delta_{jk}}, \infty)$ and when $E_{k_*}' = E_0$, then E' is a solution of the nonlinear equation

$$R_k(E_0) = x + R_j(E) - R_j(E') - R_k(\sqrt{2}\Delta_{jk} r^* - \epsilon_{jk} + E') \tag{59}$$

provided $E < E' < E_j$. Consequently, we can write

$$G_{jm}^{(1)}(x, E, E_0) =$$
$$\begin{cases} \frac{1}{2} \frac{A_j P_j(E')}{S_j(E) P_j(E)} \bar{\sigma}_{jm}(\bar{r}_*) \frac{S_m(E_0) P_m(E_0)}{S_m(\bar{r}_*) P_m(\bar{r}_*)} \text{erfc}\left(\frac{\epsilon_{jm}}{\sqrt{2}\Delta_{jm}}\right) & \text{if } E < E' < E_j \\ 0 & \text{otherwise} \end{cases} \tag{60}$$

where E' is a solution of the nonlinear equation (59), r^* is some mean value and erfc is the complimentary error function.
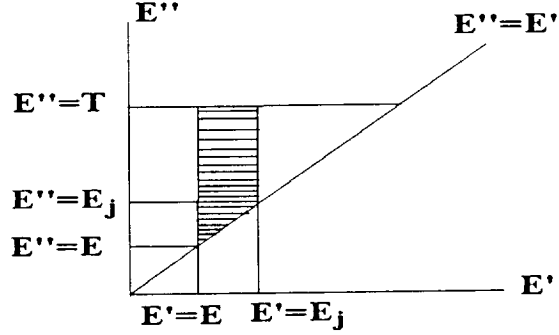
Figure 4. New limits of integration for Green's function term.

Another viewpoint

By interchanging the order of integration in equation (33) we obtain the limits of integration illustrated in the figure 4 and the equation (33) can be written as

$$
G_{jm}^{(1)}(x, E, E_0) = \int_{E}^{E_j} dE'' \int_{E}^{E''} dE' F_{jk}\delta_{km} + \lim_{T \to \infty} \int_{E_j}^{T} dE'' \int_{E}^{E_j} dE' F_{jk}\delta_{km}. \qquad (61)
$$

Observe that along the line E''=constant, we have from equation (52) that

$$
\frac{dR_k(E'_k)}{dE'_k}\frac{dE'_k}{dE'} = -\frac{dR_j(E')}{dE'}
$$

$$
\frac{A_k}{S_k(E'_k)}\frac{dE'_k}{dE'} = -\frac{A_j}{S_j(E')}
$$

$$
\text{or} \qquad dE' = -\frac{A_m S_j(E')}{A_j S_k(E'_k)}dE'_k.
$$

Hence, when $k = m$ and $\delta_{km} = 1$, the equation (61) reduces to

$$
G_{jm}^{(1)}(x, E, E_0) =
$$
$$
\int_{E_j}^{E} dE'' \int_{E_{m3}}^{E_{m1}} F_{jm}\frac{A_m S_j(E')}{A_j S_m(E'_m)}dE'_m + \lim_{T \to \infty} \int_{E_j}^{T} dE'' \int_{E''}^{E_{m1}} F_{jm}\frac{A_m S_j(E')}{A_j S_m(E'_m)}dE'_m \qquad (62)
$$

70

The limits in the above equation are determined as follows. Observe that when $E' = E$ and $k = m$ the equation (52) gives

$$
\begin{aligned}
R_m(E'_m) &= x + R_j(E) - R_j(E) + R_m(E'') \\
\text{or} \quad E'_m &= R_m^{-1}(x + R_m(E'')) = E_{m1}
\end{aligned}
$$

(63)

and when $E' = E_j$ and $k = m$ the equation (52) gives

$$
R_m(E'_m) = x + R_j(E) - R_j(E_j) + R_m(E'')
$$

. But $R_j(E_j) = x + R_j(E)$ so that $E'_m = E''$. Also when $E' = E''$ and $k = m$ we obtain from the equation (52) that

$$
\begin{aligned}
R_m(E'_m) &= x + R_j(E) - R_j(E'') + R_m(E'') \\
R_m(E'_m) &= x + R_j(E) - R_j(E'') + \frac{\nu_j R_j(E'')}{\nu_m} \\
R_m(E'_m) &= x + R_j(E) + \left(\frac{\nu_j}{\nu_m} - 1\right) R_j(E'') \\
\text{or} \quad E'_m &= R_m^{-1}(x + R_j(E) + \left(\frac{\nu_j}{\nu_m} - 1\right) R_j(E'')) = E_{m3}
\end{aligned}
$$

with

$$
E' = R_j^{-1}(x + R_j(E) - R_m(E'_m) + R_m(E'')).
$$

Using the properties of the Dirac delta function we find that the only nonzero contribution to the integral dE'_m occurs when $E'_m = E_0$. In this case the integral given by equation (62) simplifies to

$$
\begin{aligned}
G_{jm}^{(1)}(x, E, E_0) = \\
\int_{E_j}^{E} dE'' \frac{A_m S_j(E') P_j(E')}{S_j(E) P_j(E)} \sigma_{jm}(E', E'') \frac{P_m(E_0)}{S_m(E'') P_m(E'')} f_1 \\
+ \lim_{T \to \infty} \int_{E_j}^{T} dE'' \frac{A_m S_j(E') P_j(E')}{S_j(E) P_j(E)} \sigma_{jm}(E', E'') \frac{P_m(E_0)}{S_m(E'') P_m(E'')} f_2
\end{aligned}
$$

(64)

where

$$
E' = R_j^{-1}(x + R_j(E) - R_m(E_0) + R_m(E''))
$$

(65)

and

$$
f_1 = \begin{cases} 1 & \text{if } E_{m3} < E_0 < E_{m1} \\ 0 & \text{otherwise} \end{cases}
$$

(66)

$$
f_2 = \begin{cases} 1 & \text{if } E'' < E_0 < E_{m1} \\ 0 & \text{otherwise} \end{cases}
$$

(67)

71

References

[1] J.W. Wilson, F.A. Cucinotta, H. Tai, J.L. Shinn, S.Y.Chun, R.K. Tripathi and L.Sihver , *Transport of Light Ions in Matter*, Adv. Space Res. Vol.21, No. 12.,pp.1763-1771, 1998.

[2] J.W.Wilson, S.L. Lamkin, *Perturbation Theory for Charged-Particle Transport in One Dimension*, Nuclear Science and Engineering: 57, 292-299, (1975).

[3] J.W. Wilson, *Heavy Ion Transport in the Straight Ahead Approximation*, NASA Technical Paper 2178, 1983.

[4] J.W. Wilson, *Analysis of the Theory of High-Energy Ion Transport*, NASA Technical Note D-8381, 1977.

[5] S.Y. Chun, G.S. Khandelwal, J.W. Wilson, F.F. Badavi, *Development of a Fully Energy Dependent HZE Green's Function*, Proceedings of the 8th International Conference on Radiation Shielding, April 24-28, 1994, Arlington, Texas.

[6] J.W. WIlson, F.F. Badavi, *New Directions in Heavy Ion Shielding*, Proceedings of New Horizons in Radiation Protection and Shielding, published by ANS, LaGrange Park, IL, 1992, P.205.

[7] J.W. Wilson, R.C. Costen, J.L. Shinn, F.F. Badavi, *Green's Function Methods in Heavy Ion Shielding*, NASA Technical Paper 3311, 1993.

[8] J.W. Wilson, L.W. Townsend, S.L. Lamkin and B.D. Ganapol, *A Closed-Form Solution to HZE Propagation*, Radiation Research, Vol 122, 223-228, (1990).

[9] J.L. Shinn, J.W. Wilson, W.Schimmerling, M.R. Shavers, J.Miller, E.V. Benton, A.L. Frank, F.F. Badavi, *A Green's Function Method for Heavy Ion Beam Transport*, Radiation Environment Biophysics, Vol. 34, 155-159, (1995).

[10] J.W. Wilson, F.F. Badavi, J.L. Shinn, R.C. Costen, *Approximate Green's Function Methods for HZE Transport in Multilayered Materials*, NASA Technical Memorandum 4519, 1993.

[11] S.Y. Chun, G.S.Khandelwal, J.W.Wilson, *A Green's Function Method for High Charge and Energy Ion Transport*, Nuclear Science and Engineering, Vol. 122, 267-275, (1996).